



University of North Dakota
UND Scholarly Commons

Theses and Dissertations

Theses, Dissertations, and Senior Projects

January 2013

Evaluating The Impact Of Above-Cloud Aerosols On Cloud Optical Depth Retrievals From Modis

Ricardo Alfaro

Follow this and additional works at: <https://commons.und.edu/theses>

Recommended Citation

Alfaro, Ricardo, "Evaluating The Impact Of Above-Cloud Aerosols On Cloud Optical Depth Retrievals From Modis" (2013). *Theses and Dissertations*. 1499.

<https://commons.und.edu/theses/1499>

This Thesis is brought to you for free and open access by the Theses, Dissertations, and Senior Projects at UND Scholarly Commons. It has been accepted for inclusion in Theses and Dissertations by an authorized administrator of UND Scholarly Commons. For more information, please contact zeinebyousif@library.und.edu.

EVALUATING THE IMPACT OF ABOVE-CLOUD AEROSOLS ON CLOUD OPTICAL
DEPTH RETRIEVALS FROM MODIS

by

Ricardo Alfaro
Bachelor of Arts, University of Colorado, 2010
Master of Science, University of North Dakota, 2013

A Thesis

Submitted to the Graduate Faculty

of the

University of North Dakota

in partial fulfillment of the requirements

for the degree of

Master of Science

Grand Forks, North Dakota
December
2013

Copyright 2013 Ricardo Alfaro

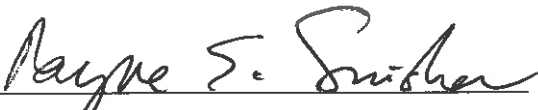
This thesis, submitted by Ricardo Alfaro in partial fulfillment of the requirements for the Degree of Master of Science from the University of North Dakota, has been read by the Faculty Advisory Committee under whom the work has been done and is hereby approved.



Chairperson



This thesis is being submitted by the appointed advisory committee as having met all of the requirements of the School of Graduate Studies at the University of North Dakota and is hereby approved.



Dr. Wayne Swisher
Dean, School of Graduate Studies



Date

PERMISSION

Title EVALUATING THE IMPACT OF ABOVE-CLOUD AEROSOLS ON CLOUD
OPTICAL DEPTH RETRIEVALS FROM MODIS

Department Atmospheric Sciences

Degree Master of Science

In presenting this thesis in partial fulfillment of the requirements for a graduate degree from the University of North Dakota. I agree that the library of this University shall make it freely available for inspection. I further agree that permission for the extensive copying for scholarly purposes may be granted by the professor who supervised my thesis work or, in their absence, by the chairperson for the department or the dean of the Graduate School. It is understood that any copying of publication or other use of this thesis or part thereof for financial gain shall not be allowed without my written permission. It is also understood that due to recognition shall be given to me and to the University of North Dakota in any scholarly use which may be made of any material in my thesis.

Name: Ricardo Alfaro

Date: 12/12/2013

TABLE OF CONTENTS

LIST OF FIGURES	vii
LIST OF TABLES	ix
ACKNOWLEDGEMENTS	x
ABSTRACT	xi
CHAPTER	
I. INTRODUCTION	1
II. DATA	7
Modis Algorithm Description.....	7
Omi Algorithm Description.....	12
CALIOP Algorithm Description.....	15
III. METHODS	18
Collocation of Data Sets.....	18
Data Filtering.....	19
IV. RESULTS AND DISCUSSIONS	23
Global Distribution.....	23
A Case Study.....	27
Seasonal and Regional Impacts.....	28
Passive Remote Sensing	28
Active Remote Sensing.....	33
V. SUMMARY AND CONCLUSION.....	38

APPENDIX	42
References.....	43

LIST OF FIGURES

Figure	Page
<p>1. Two year (2007-2008) spatial plot (a) seasonal Ozone Monitoring Instrument (OMI) Aerosol Index (AI) over cloudy scenes during the summer season (June, July, August or JJA) for 2007 and 2008 combined, (b) The seasonal OMI AI average over Moderate Resolution Imaging Spectroradiometer (MODIS) cloudy scenes during the spring season (March, April, May or MAM) for 2007 and 2008, (c) frequency of occurrence of above-cloud aerosols ($AI > 1$) for the summer of 2007 and 2008, (d) same as 1c for the JJA of 2007-2008.....</p>	26
<p>2. Case study of collocated Ozone Monitoring Instrument (OMI) and Aqua Moderate Resolution Imaging Spectroradiometer (MODIS) on August 4th, 2007 at 13:00 UTC. Top left corner shows the MODIS true color image off the southwest coast of Africa. The red line visible in the image is the Cloud-Aerosol Lidar with Orthogonal Polarization (CALIOP) overpass. The top middle diagram depicts the Ozone Monitoring Instrument Aerosol Index (OMI AI), retrieved from collocated MODIS data set, for the same area as the MODIS true color image. Top right figure corner figure shows the cloud top temperature from MODIS for the same area as MODIS true color image. The vertical CALIOP backscatter can be seen, figure in second row, confirming the presence of an aerosol plume suspended over a low level cloud. Figure in the third two to the left shows the cloud optical depth (COD) using the standard MODIS COD data aggregated into a 5 km product. Middle plot on the third row shows the COD retrieval using the supplementary MODIS COD data. Right figure on third row shows the difference in COD retrievals (standard vs. supplementary) using only valid pairs of COD data. The last row shows the standard effective radius retrievals, supplementary retrievals and difference in retrievals, respectively, similar to COD in units of microns.....</p>	29
<p>3. Scatter plot of Ozone Monitoring Instrument (OMI) Aerosol Index (AI) vs. binned averaged difference between retrieved standard and supplementary cloud optical depth (ΔCOD) from Moderate Imaging Resolution (MODIS) as a function of COD (a) for the ‘smoke outflow’ region ($22^{\circ} S - 5^{\circ} N$ and $18^{\circ} W - 15^{\circ} E$) for June-August, 2007, (b) for the ‘dust outflow’ region ($5^{\circ} N - 30^{\circ} N$ and $60^{\circ} W - 16^{\circ} W$) during June-August, 2007, (c) for the ‘smoke outflow’ region of June-August 2008 and (d) for the ‘dust outflow’ region for June-August 2008.....</p>	31
<p>4. Scatter plot of Ozone Monitoring Instrument (OMI) Aerosol Index (AI) vs. binned averaged difference between retrieved standard and supplementary cloud optical depth (ΔCOD) from Moderate Imaging Resolution (MODIS) as a function of COD separated</p>	

into early months of the biomass burning season July and August – solid line) and later burning months (September and October dotted line) over ‘smoke outflow’ region(22° S – 5° N and 18° W - 15° E) during the (a) the 2007 biomass burning season and (b) during the 2008biomass burning season33

5. Scatter plot of Ozone Monitoring Instrument (OMI) Aerosol Index (AI) vs. binned averaged difference retrieved standard and supplementary cloud optical depth (Δ COD) from Moderate Resolution Imaging Spectroradiometer (MODIS) for the Gulf of Tonkin region off the coast of Northern Vietnam (7°N - 25°N and 105°E - 120°E) during the early spring dust storms months (February, March, April or FMA) for (a) 2007 and (b) 2008.....34
6. Scatter plot of Ozone Monitoring Instrument (OMI) Aerosol Index (AI) vs. Cloud-Aerosol Lidar with Orthogonal Polarization (CALIOP) above-cloud AOD as a function of the underlying Moderate Resolution Imaging Spectroradiometer (MODIS) COD during the summer of 2007. The AI are binned into 0.1 increments while the AOD are binned into 0.01increments and the COD are binned as shown in plot. (a) shows the relationship for the smoke outflow region while (b) shows the relation for the dust outflow region.....35
7. Relationship between above-cloud Cloud-Aerosol Lidar with Orthogonal Polarization (CALIOP) AOD and binned averaged difference between retrieved standard and supplementary cloud optical depth (Δ COD) from Moderate Imaging Resolution (MODIS) during the 2007 summer (a) over the smoke outflow region (b) between Ozone Monitoring Instrument (OMI) Aerosol Index (AI) with CALIOP restraints and Δ COD for smoke outflow region and (c) relationship between CALIOP AOD and Δ COD. The cod range of 16-20 is removed from figure 7c due to limited number of collocated CALIOP pixels and high amounts of noise36

LIST OF TABLES

Table	Page
1. MODIS cloud mask decision tree. Each pixel is subject to the test described in Table 1. In order for a cloud to be considered cloudy, the pixel must pass all of the tests listed.	9

ACKNOWLEDGEMENTS

Thank you to my advising committee of Drs. Jianglong Zhang, Cedric Grainger and David Delene for their continual guidance and support throughout the course of this thesis work. Gracias a mi familia en Denver por todo el apoyo e ayuda que me han dado durante esta epoca dificil di mi vida especialmente con mi nuevo hijo Richie. Thank you to my fatty, April, for being by my side all of these years and being a great mom to our son. Thank you to all of my friends and colleagues for their encouragement, help and support during this process. Thank you to all of the graduate students in the Atmospheric Sciences Department for the fun times and long nights at the office doing research and homework. Special thanks to Yinqxi Shi, Randall Johnson and Travis Toth for their help and advice with computer programming and data processing.

The North Dakota Space Grant Consortium funded this research. The CALIPSO data (Drs. David Winkler and Mark Vaughn) were obtained from the NASA Langley Center for Atmospheric Research Science Data Center. The MODIS data were obtained from NASA Goddard Space Flight Center. The OMI data were obtained from Goddard Earth Science Data and Information Service Center. Dr. James Campbell is thanked for providing some of the figures and for his expertise and guidance.

ABSTRACT

Using two different operational Aqua Moderate Resolution Imaging Spectroradiometer (MODIS) cloud optical depth (COD) retrievals (visible and shortwave infrared), the impacts of above-cloud absorbing aerosols on the standard COD retrievals are evaluated. For fine-mode aerosol particles, aerosol optical depth (AOD) values diminish sharply from the visible to the shortwave infrared channels. Thus, a suppressed above-cloud particle radiance aliasing effect occurs for COD retrievals using shortwave infrared channels. Aerosol Index (AI) from the spatially and temporally collocated Ozone Monitoring Instrument (OMI) are used to identify above-cloud aerosol particle loading over the southern Atlantic Ocean, including both smoke and dust from the African sub-continent. MODIS and OMI Collocated Cloud-Aerosol Lidar and Infrared Pathfinder Satellite Observations (CALIPSO) data are used to constrain cloud phase and provide contextual above-cloud AOD values. The frequency of occurrence of above-cloud aerosols is depicted on a global scale for the spring and summer seasons from OMI and CALIOP, thus indicating the significance of the problem. Seasonal frequencies for smoke-over-cloud off the southwestern Africa coastline reach 20-50% in boreal summer. We find a corresponding low COD bias of 10-20% for standard MODIS COD retrievals when averaged OMI AI are larger than 1.0. No such bias is found over the Saharan dust outflow region off northern Africa, since both MODIS visible and shortwave infrared channels are vulnerable to dust particle aliasing, and thus a COD impact cannot be isolated with this method. A similar result is found for a smaller domain, in the Gulf of Tonkin region, from smoke advection over marine stratocumulus clouds and outflow into the northern South China Sea in spring. This study shows

the necessity of accounting for the above-cloud aerosol events for future studies using standard MODIS cloud products in biomass burning outflow regions, through the use of collocated OMI AI and supplementary MODIS shortwave infrared COD products.

CHAPTER I

INTRODUCTION

Clouds strongly modulate the energy balance of the Earth and its atmosphere through their interaction with long-wave terrestrial and short-wave solar radiation, as demonstrated from satellite observations (Ramanathan et al., 1987). However, cloud distribution varies considerably in the vertical and horizontal directions, due to the circulation patterns of atmospheric downdrafts and updrafts. Thus, knowledge of cloud properties and their spatial and temporal variability is crucial to the study of global circulation models (GCM) along with climate monitoring and modeling (Wetherald and Manabe 1988, modis-atmos.gsfc.nasa.gov).

Satellite sensors, such as the Moderate Resolution Imaging Spectroradiometer (MODIS), can passively measure radiances in the visible and near-infrared regions of the electro-magnetic spectrum, hence making satellite sensors important tools to aid in understanding the role of cloud systems in the Earth's radiation budget (Painemal and Zuidema, 2011). In particular, the cloud optical depth (COD) and cloud effective radius (r_e) parameters are retrieved based on the observed top-of-atmosphere (TOA) spectral radiance from cloudy scenes (King et al., 1997). The unique capabilities of passive sensors with wide swaths allow for measurements of TOA spectral radiances with near daily global coverage.

The cloud property retrieval algorithms for passive satellite remote sensing are based on certain assumptions with respect to realistic conditions in the atmosphere. For example, the

MODIS retrieval algorithms assume vertically uniform plane parallel clouds where in reality, the clouds are typically vertically stratified and horizontally inhomogeneous (Min et al. 2012). Such assumptions can lead to errors due to ; the MODIS solar/satellite viewing geometries and the associated three-dimensional radiative effects (Marshak et al. 2006; Vant-Hull et al. 2007; Kato and Marshak, 2009), variations of the satellite scanning angle and its effects on sub-pixel clear sky contamination (Maddux et al. 2010), and the attenuation of the upwelling cloud radiance by above-cloud aerosols (Coddington et al. 2010; Haywood et al. 2004) which may affect the satellite retrieved cloud properties.

The impacts of above-cloud aerosols to conclusions in various cloud studies are not unknown. Haywood et al. (2004) investigated the impacts of partially absorbing above-cloud biomass burning and mineral dust aerosols on MODIS cloud property retrievals using coincident in-situ observations from the Southern African Regional Science Initiative (SAFARI) and Saharan Dust Experiment (SHADE) missions. Analysis of 1 km resolution MODIS data during SAFARI suggests that MODIS derived cloud properties, COD and r_e , are subject to a low bias in the presence of overlying biomass burning aerosols, thus reducing the level of certainty for such retrievals.

Similar to the Haywood et al (2004), Coddington et al. (2010) performed an inter-comparison during the 2004 Intercontinental Chemical Transport Experiment near Portsmouth, New Hampshire. Solar spectral flux radiance measurements taken above and below an aerosol layer atop a cloud layer were compared to MODIS-retrieved COD and r_e . The remotely sensed COD were biased low in the presence of absorbing aerosols while non-absorbing aerosols had no impact on the MODIS retrievals similar to the results found in Haywood et al. (2004) study. In situ measurements provide accurate results and at times serve as a benchmark for remote sensing

measurements however, such experiments are limited in spatial coverage. Thus, remote sensing techniques that can provide global data on a daily basis are needed for a long-term climatological study of above-cloud aerosols.

Wilcox et al. (2009) conducted a remote sensor study utilizing measurements from several spectral channels in order to investigate the indirect impact of above-cloud aerosols on COD retrievals. MODIS liquid water path (LWP), derived from the product of COD and r_e , was compared with LWP microwave retrievals, over the ocean, from the Advanced Microwave Scanning Radiometer - Earth Observing System (AMSR-E). Sub-micron sized aerosols are transparent at microwave wavelengths and hence do not affect LWP retrievals. Similar to the results from in situ studies, LWP from MODIS were biased low in the presence of absorbing aerosols when compared to AMSR-E retrievals during the biomass burning seasons of 2005 and 2006 off the Atlantic Coast of southern Africa. However, LWP is not a direct measure of COD and contains unconstrained information for both COD and r_e . Furthermore, LWP estimates from AMSR-E have their own limitations (e.g. Seethala et al. 2010). Meyer et al. (2013) located above-cloud aerosols using Cloud-Aerosol Lidar with Orthogonal Polarization (CALIOP) measurements and attempted to correct for their effects on retrieved cloud properties using a look-up-table (LUT) approach during the biomass burning season in Southern Africa. Similar to Wilcox et al (2009), the cloud top properties, COD and r_e , were biased low in the presence of above-cloud aerosols. However, CALIOP covers a small portion of the swaths from passive sensors such as MODIS, and methods that can expand the correction to a full MODIS swath are needed. This problem is well recognized however the quantitative impact of above-cloud aerosol presence on passive COD retrievals has not been estimated for global application nor have solutions been proposed to improve cloud property retrievals that account for this effect on a

large spatial scale. The primary reason for this is the aliasing problem that develops when trying to decouple aerosol and cloud radiances from passive measurements. The over-whelming reflectance from the underlying cloud makes it very difficult to measure the drastically smaller aerosol reflectance, which is a major source of uncertainty when using the visible channel to detect above-cloud aerosols (e.g. Remer et al. 2005; Kahn et al. 2012).

Combined measurements from Aqua MODIS, Ozone Monitoring Instrument (Torres et al. 1998) and CALIOP (Winker et al. 2010) in the NASA A-train satellite constellation provide an opportunity for estimating COD uncertainties derived from passive sensors in the presence of aerosols above cloud top. The Ozone Monitoring Instrument (OMI) on board the AURA satellite uses measurements in the near-UV region in order to infer the presence of absorbing aerosols in cloud free and cloudy scenes. The detection of aerosol characteristics using near-UV observations during clear sky conditions is a well-established remote sensing technique originally used on the Total Ozone Mapping Spectrometer (Torres et al. 1998). Utilizing the near-UV detection method, previously used on other sensors such as Global Ozone Monitoring instruments, GOME and GOME-2, and Scanning Imaging Absorption spectrometer for Atmospheric Cartography, allows for the detection of absorbing aerosols even over bright backgrounds such as snow, ice, and clouds. However, the improved spatial resolution and increased number of observed wavelengths from OMI sets a new standard for trace gas and air quality monitoring from space.

The MODIS operational product, MYD06, offers two types of cloud optical property retrievals, which are the standard COD and r_e retrievals based on the combined observations from visible and near-IR channels (0.86, 1.6, 2.16 and 3.7 μm) and the supplementary COD and r_e retrievals using two shortwave infrared channels (1.6 and 2.1 μm). It is interesting to compare

COD values for the two products, as the COD retrievals from the standard MODIS cloud products are mostly dependent upon observations at the 0.86 μm channel (over ocean), while the COD values from the supplementary shortwave infrared product are derived using the 1.6 μm channel. In comparison, while both the 0.86 and 1.6 μm channels are sensitive to the presence of large aerosols such as dust aerosols, the sensitivity of smoke plumes drastically diminishes from the 0.86 μm to the 1.6 μm channels (Remer et al. 2005). Thus, with the use of colocated OMI AI and COD data from both MODIS standard and supplementary products, the impacts of above-cloud aerosols to MODIS COD data can be directly evaluated at near full Aqua MODIS swath.

OMI AI values above-cloud are only semi-quantitative since optically reflective clouds may anomalously raise the value relative to any substantive changes in above-cloud aerosol particle mass loading. A recent study by Yu et al., (2011) found a highly linear relationship between the above-cloud OMI AI and CALIOP AOD over both smoke and dust aerosol polluted regions, indicating that OMI AI can be used, effectively, as an indicator for the presence of UV-absorbing aerosols above clouds. Still, as mentioned in Yu et al., (2011), the OMI AI and CALIOP AOD relationship is also a function of COD and aerosol type which needs to be taken into consideration in this study. In order to aid the OMI-MODIS analysis, it is necessary to include AOD data which are independent of aerosol type and underlying COD. Thus, above cloud AOD from CALIOP is also used for evaluating the impacts of above-cloud aerosols to COD retrievals as well as validating results from our passive sensor study.

The OMI AI has a strong dependence on single scattering albedo (SSA) of the aerosols, which is defined as the ratio of the scattering efficiency to the total extinction efficiency. In particular, a recent study by Eck et al. (2013) that utilized 15 years of Aerosol Robotic Network

(AERONET) data found an increase in smoke aerosol SSA (decrease in aerosol absorption) from July to November over much of the South Africa region. Therefore, it is essential to compare biomass burning season effects on cloud property retrievals during the early part of the burning season with those of the later months in order to determine the effects a varying SSA (absorption) will have on the OMI AI measurements.

The goal of this study is to build upon previous studies by examining the impacts of absorbing aerosols, detected by the OMI algorithm, on retrieved cloud properties from passive space-borne sensors. While there are other possible contaminants, which can affect the cloud property retrievals, this study focuses on above-cloud absorbing aerosols. The impact of above-cloud aerosols on cloud property retrievals is first evaluated using collocated space-borne observations from passive sensors, followed by the use of collocated data from the active sensor, CALIOP, in order to verify the results of the passive sensor study. The following research questions are addressed:

- (1) What kind of seasonal variability is seen in absorbing aerosols over low level stratocumulus clouds over oceans?
- (2) Does the use of active and passive based satellite sensor allow us to examine the impacts of above-cloud absorbing aerosols on instantaneous and/or climatological cloud property retrievals?
- (3) Will the dependencies of OMI AI on SSA and COD affect OMI AI's use for this study?
- (4) Do results from the CALIOP vertical profile agree/disagree with the results of the study utilizing MODIS and OMI?

CHAPTER II

DATA

Three data sets are used for this study: (1) OMI Level 2 Orbital Swath Collection 3-OMAERUV, (2) MODIS/Aqua Level 2 Collection 5 cloud fraction and cloud optical depth-MYD06, and (3) CALIOP Cloud and Aerosol Layer Products. Both, OMI and MODIS have wide swaths of 2600 and 2330 km; respectively, which allows for full global coverage on a daily basis. The OMI data set serves as an indicator of the presence of absorbing aerosols however due to the bias COD creates on AI retrievals, the CALIOP AOD is also used in order to validate the results from the OMI AI. MODIS provides COD and r_e retrievals at two separate spectral bands. The data sets are described in the following section.

MODIS Algorithm Description

The Moderate Resolution Imaging Spectroradiometer (MODIS) on board the Aqua satellite (local equator crossing time of 1:30 PM) provides high spatial resolution of 250-1000 meters at 36 different spectral channels. Its wide swath of 2330 km covers the entire globe twice a day. MODIS orbits in a linear formation with several other satellites as part of the A-train constellation of satellites. Several wavelengths, ranging from the visible channels to the infrared channels (IR) are used in cloud detection, cloud mask, and cloud optical property retrievals in order to generate level 2 cloud products. Level 2 MODIS cloud products are available at 1 km and 5 km spatial resolution. The MODIS Cloud Product combines IR and visible techniques to determine radiative cloud properties such as COD and r_e .

For this study, the collection 5 MODIS cloud products, MYD06, products over cloudy ocean retrievals are used. Comparing with the previous version of the MODIS cloud products, improvements have been made to the collection 5 MODIS cloud products including improved cloud phase algorithm, improved ice libraries, new clear sky restoral algorithm (which helps filter aerosol and sun glint contamination), and new surface albedo maps (King et al. 2006). Another difference from the previous version the MODIS cloud product is the supplementary retrievals to be used with the standard retrievals for this study. Cloud fraction is used, given by the percentage of cloud mask pixels determined to be cloudy within a 5 km MODIS scene, to find the percentage of cloud cover over a 5 km MODIS scene. The standard and supplementary retrievals of r_e and COD from the MYD06 MODIS/Aqua product are the parameters which are compared against each other.

The cloud fraction parameter, sampled at a 5 km spatial resolution, is directly derived from the 1 km sampled MOD35 Cloud Mask product. Multispectral analysis from more than a dozen MODIS bands along with a decision tree analysis determine whether each 1 km MODIS pixel is either cloudy or clear. The decision tree analysis is shown below in Table 1, which describes each of the tests performed on every single MODIS pixel in order to determine whether the pixel is cloudy. In order to be considered cloudy, the individual pixel must pass all the tests described below. The 1 km cloud mask product is then binned into a 5 km product where the cloud coverage fraction is determined from the number of cloudy pixels within the sampled area. Other ancillary parameters such as quality assurance (QA), geo-location information, and scan times are copied directly from the cloud mask product directly into the cloud fraction parameters.

Table 1. MODIS cloud mask decision tree. Each pixel is subject to the test described in Table 1. In order for a cloud to be considered cloudy, the pixel must pass all of the tests listed.		
<i>Test Name</i>	<i>Method</i>	<i>Surface Type</i>
<i>IR Threshold</i>	$T_{IR} < T_S - 2K$ $T_{IR} = IR \text{ temperature}$ $T_S = \text{surface temperature}$	All
<i>Spatial Coherence</i>	$\sigma > 0.2 K$ $\sigma > 1K$ <i>Find standard deviation of 3x3 surrounding pixels</i>	Ocean Land
<i>Visible Threshold</i>	$R > R_S + \Delta R$ $R_S = \text{surface reflectance}$ $\Delta R = \text{difference in reflectance between surface and detected object in the visible channels}$	$\Delta R \sim 3\%$ Ocean $\Delta R \sim 6\%$ Land $\Delta R \sim 15\%$ Coasts
<i>Channel Ratio</i>	$Q = R_{0.86} / R_{0.65}$	$Q \sim 1$ clouds $Q < 1$ ocean $Q > 1$ land
<i>Thin Cirrus</i>	<i>Utilizes the 1.38 μm band in order to infer the presence of thin cirrus clouds</i>	All

The COD and r_e are known for a given set of viewing geometries and radiances retrieved from a radiative transfer model, which are then used to build LUTs. MODIS measured radiances, which are a function of viewing geometries; solar zenith angle (SZA), viewing zenith angle (VZA) and relative azimuth angle, are inserted into the LUT. The COD and r_e are determined simultaneously by comparing the measured reflectance and searching for the combination of COD and r_e which gives the best fit for the given set of viewing geometries (Twomey and Cocks, 1982,1989). A different LUT exists for every combination of the three viewing geometries. The large number of interpolations required for each of the above variables creates sorting and computational inefficiencies for optically thicker clouds (King et al. 2006), therefore an alternate method was suggested by Nakajima and King (1990). Nakajima and King

applied asymptotic theory to optically thick clouds which greatly reduced the number of LUT computations needed thus decreasing the inefficiencies during the interpolation process.

When the optical thickness of the atmosphere is sufficiently large, numerical results must agree with the asymptotic expressions for very thick layers (van de Hulst 1980). The asymptotic theory suggests that the reflection of an optically thick cloud depends on the asymmetry factor and the SSA of a small volume cloud of air as well as the terrestrial surface albedo. The effective radius is defined by

$$r_e = \int_0^\infty r^3 n(r) dr / \int_0^\infty r^2 n(r) dr \quad (1)$$

where $n(r)$ is the particle size distribution and r is the radius of the particle. However, the r_e in the LUT approach assumes no dependence on cloud particle size distribution which may lead to some uncertainties in the r_e retrievals. Nakajima and King (1990) showed that the asymmetry parameter and hence the cloud optical thickness of optically thick clouds may be affected in making assumptions about the cloud particle size distribution. Validation of MODIS retrieved cloud physical and optical properties are conducted through comparisons of other remote sensing platforms such as GOES and lidar measurements along with aircraft measurements (modis-atmos.gsfc.nasa.gov). MODIS retrieved COD is found to be well correlated with in situ derived COD while MODIS retrieved r_e and LWP were found to systematically exceed in situ cloud top values by about 20% (Painemal et al. 2011).

The COD and cloud r_e retrieved from remote sensing techniques are based on the underlying principle that reflection of clouds at a non-absorbing band in the visible wavelength region is primarily a function of COD while the reflection within a water or ice absorbing band in the near IR is a primarily a function of r_e (King et al. 2007). The COD and r_e retrievals are intended for plane-parallel liquid water clouds and it is assumed that all MODIS data analyzed

by the algorithm have been screened by the cloud mask of Ackerman et al. (1997) (King et al. 1997). The Standard MODIS product uses spectral bands centered at a visible wavelength (0.645 μm) and three near-IR wavelengths (1.64, 2.13 and 3.75 μm) which are used in the daytime shortwave cloud retrieval algorithm over a land surface. For ocean retrievals, the visible band is replaced by a MODIS band centered at 0.858 μm . In addition to the standard products, a new supplementary cloud optical property retrieval using bands six and seven (1.6 and 2.1 μm) was added to MODIS collection 5. The new retrieval, computed only for clouds over ocean and snow/ice surfaces, is performed with comparisons to the standard MODIS cloud optical property retrievals. All land retrievals lacking snow and ice contain fill values in the supplementary product which restricts this study to over oceans scenes. It should be noted that the supplementary retrievals are also applied to deep inland rivers and lakes. The supplementary MODIS product has data gaps due to the damaged 1.6 μm detector. Thus, a correction algorithm based on training data was proposed in order to successfully replace the missing data (Gladkova et al. 2011). However, only MODIS pixels with valid supplementary and standard cloud top property retrievals are used. Higher values of MODIS cloud retrievals of COD and r_e are observed near the edge of the swaths due to factors such as larger pixel size and a longer path length at more oblique sensor zenith angles which are not readily apparent when averaging multiple satellite overpasses over the entire globe (Maddux et al. 2010).

The data sets containing cloud optical properties and geolocation information are the MYD06_L2 Cloud Products and MYD03_L3 geolocation retrieved from the MODIS sensor on board the Aqua platform. The MYD06 data sets represent cloud properties and geolocation information at different spatial resolutions. Parameters such as the geolocation information such as latitude, longitude and pixel scan time along with cloud fraction and cloud top temperature are

all sampled at a 5 km resolution. Cloud optical and physical properties such as COD, r_e , and LWP are all sampled at 1 km resolution which are available from the standard retrieval products (Cloud_Optical_Thicknes, Cloud_Effective_Radius, and Cloud_Water_Path) and the supplementary retrieval products (Cloud_Optical_Thicknes_1621, Cloud_Effective_Radius_1621, and Cloud_Water_Path_1621). QA flags are available for each of the optical and physical cloud parameters along with the cloud fraction. It should be noted that the cloud fraction and cloud fraction QA are based on the Cloud Mask Product described previously.

Geolocation information retrieved from the cloud product data is not sampled at the same spatial resolution as the cloud properties and thus, cloud property retrievals do not contain unique geolocation information but instead share the same location with the surrounding pixels. This proved to be an issue while performing an inter-sensor comparison with a nadir scanning instrument such as CALIOP. Therefore, the MYD03 product is used to provide us with a unique location in space and time for each and every one of our 1 km cloud property retrievals.

The QA flag separates scenes according to the confidence in their retrievals. Each parameter contains its own QA flag but are all separated into four different levels of confidence: (1) No confidence or fill values, (2) Marginal Confidence, (3) Good Confidence, and (4) Very Good Confidence. Negative values of all cloud properties are reported in the MODIS collection 5 cloud products and are considered fill values which can be removed by using the QA flags.

Omi Algorithm Description

OMI is a nadir-viewing near UV/Visible Charge Coupled Device (CCD) spectrometer onboard Aura. Aura is the trailing satellite in the A-Train constellation of satellites, lagging the Aqua satellite by approximately 15 minutes. The orbit has an altitude of 705 km with a local equator

crossing time of 1:45 PM. OMI measurements cover a spectral region from 0.264-0.504 μm with a spectral resolution between 0.00042 and 0.00063 μm . The 2600 km wide swath enables global coverage on a daily basis with a footprint of 13x24 km at nadir, which varies to 28x150 km at the extremes of the swath. The OMI instrument works in three different modes; global mode, spatial zoom-in mode and spectral zoom-in mode. The global measurement mode is the default mode which samples the complete swath over the entire wavelength range. The spatial and spectral zoom-in modes have a ground pixel size of 13x12 km at nadir. The spatial zoom-in mode has a limited swath width with a spectral band covering 0.264-0.311 μm and is used once every 32 days always above the same geolocations. The spectral zoom mode covers the entire 2600 km swath but has limited spectral coverage in the near UV ranging from 0.307-0.432 μm . Since this study is only concerned with default global mode in the near UV and visible spectrum, the other two modes will henceforth not be discussed in detail any further.

The OMI products are available at four separate levels; Level 0, level 1B, level 2, and level 3. OMI level 2 products contain geophysical parameters derived from daytime level 1b radiometrically geolocated radiances (OMI team, 2012). In addition to the standard derived parameters, the level 2 files also contain auxiliary data such as viewing geometries and ground pixel quality flags.

The OMAERUV algorithm utilizes measurements in the near UV at two different wavelengths, 0.354 and 0.388 μm , in order to take advantage of the sensitivity of the large upwelling radiation absorbed by aerosols in this spectral region. There are two advantages for deriving the presence of aerosols in the near UV region. First, objects which are bright in the visible spectrum such as deserts, snow, ice and clouds are not very bright in this spectral region. The second advantage is the strong interaction between aerosol absorption and molecular

scattering from below the aerosols which allows for the estimation of the aerosol loading in the atmosphere (Torres et al. 2007).

AI is used to determine the amount of aerosol loading above the bright backgrounds. In order to calculate the AI, the first step is to use a radiative transfer model (RTM) that assumes pure Rayleigh scattering and an opaque Lambertian reflector bounding the atmosphere in order to compute the radiance at 0.388 μm . In order to compute the radiance at 0.354 μm , the radiance at 0.388 μm is corrected for the spectral dependence of surface reflectivity using a pre-computed climatology database (Torres et al. 2007). Equation 2 gives the definition for the Aerosol Index.

$$AI = 100 * [\log(\frac{I_{0.388}}{I_{0.354}})_{measured} - \log(\frac{I_{0.388}}{I_{0.354}})_{calculated}] \quad (2)$$

where $I_{measured}$ is the radiance measured from the OMI sensor and $I_{calculated}$ is the radiance retrieved from the RTM which assumes a perfect atmosphere free of absorbing aerosols. AI is a residual quantity which calculates the difference between the calculated and measured ratios of absorbing and non-absorbing spectral channels. Positive AI values generally indicate absorbing aerosols while small or negative values represent non-absorbing aerosols and clouds. It is important to note that the AI is not an exclusive measurement of aerosol loading but also depends on other parameters such as index of refraction, particle size distribution, the height of the aerosol layer and the underlying cloud thickness. Nevertheless, AI was found to have a linear relation with AOD which depends on COD and aerosol type (Yu et al. 2011).

The level-2 OMI near UV Aerosol Optical Depth (OMAERUV) version 3 data set provides the derived AI parameter along with all necessary ancillary data such as the geolocation, QA flags, and viewing geometry parameters. Due to the large OMI footprint, especially away from nadir, the OMI ground pixel corner product (OMPIXCOR) is used in order to determine the coordinates of the corners of the OMI pixel. The QA parameter separates each

OMI scene according to the quality of the retrieval. The QA flag filters individual OMI scenes which may be contaminated by snow and/or ice, have a SSA or AOD not within thresholds, may be contaminated by sun glint effects ($\text{SZA} > 70^\circ$), contain a terrain pressure not within acceptable bounds or contained a cross track anomaly. Not all flags are applicable to this study and the flags of interest will be discussed in detail in the methodology section.

Caliop Algorithm Description

Active remote sensors such as Radio Detecting and Ranging (RADAR) and Light Detecting and Ranging (LIDAR), transmit pulses of energy at particular wavelengths (Purkis and Klemas 2011). Active remote sensing is useful because unlike nadir-viewing passive sensors, active sensors provide direct vertical measurements of atmospheric properties but with more limited spatial coverage than their passive sensor counterparts. CALIOP onboard CALIPSO utilizes a LIDAR pulse and has been used in the past in order study above-cloud aerosol events (Yu et al. 2011).

Level 2 algorithms are divided into three modules which serve to detect layers, classify the layers by type, and perform extinction retrievals. The combination of the three modules allows for the detection of weak features that lie beneath strong features using a dynamic threshold technique (Vaughan et al. 2004). It estimates the optical layer optical depths, which are then used to correct the signal attenuation for overlying features. When a feature is first detected, it is identified as either cloud or aerosol by the Scene Classification Algorithm (SCA) depending on the scattering strength of the feature (usually clouds scatter more intensely than aerosol plumes). If the layer is classified as a cloud then the SCA will determine if it is composed of water or ice utilizing a layer-average depolarization ratio along with ancillary data such as layer height and temperature (Hu et al. 2011). The SCA also chooses an appropriate

lidar ratio required to retrieve derived parameters such as aerosol or cloud optical depth. The final computation of the optical depths is performed by the Hybrid Extinction Retrieval Algorithms (HERA) which averages a varying number of profiles in a grid to produce a single attenuated backscatter profile which is used by the layer classification algorithm.

CALIPSO level 2 data are separated into three products (CALIPSO Data Products Catalog 2006): layer products, profile products, and the vertical feature mask (VFM). The profile products contain the retrieved extinction and backscatter profiles within the aerosol and cloud layers detected by CALIOP. Profile products are reported at a 5 km horizontal resolution and a 60 m vertical resolution over an altitude range from 20 km down to -0.5 km for the cloud product while the aerosol product extends up to 30 km in altitude. Layer products are binned into a horizontal resolution of 5 km whereas the vertical resolution is determined by the vertical distribution of the feature detected in any given layer. Layer products contain layer-integrated cloud/aerosol properties along with ancillary parameters for each CALIOP detected layer. The range of altitudes is similar to the profile products for both aerosol and clouds. The VFM is a feature classification product that provides information on the location and type of aerosols and clouds within CALIOP retrievals (Winker et al. 2012). It can be used to discriminate the feature identified in the layer product (i.e. aerosol vs. cloud) and their column distributions which allows for optimal layer detection and characterization (Vaughan et al. 2009).

Only layer products are used in this study, thus the profile products and VFM will no longer be discussed in detail. Daytime, version 3.01 Level 2, 5 km Aerosol Layer (L2_05kmALay) and Cloud Layer (L2_05kmClay) products are used for this study. The cloud layer product is used to find the vertical distribution of clouds while the total column AOD is calculated from the individual layers of integrated AODs from the aerosol layer products. The

QA parameter 'Feature Finder QC' is used in order to ensure only data which is of good quality is utilized. The CALIOP AOD is validated against the U.S. Naval Aerosol Analysis and Predictive System (NAAPS), which features a two-dimensional variational assimilation of NASA MODIS and Multi-angle Imaging Spectroradiometer (MISR) quality-assured datasets, combined with regional ground-based lidar measurements. CALIOP AOD retrievals are biased low over open water relative to NAAPS retrievals possibly due to the a-priori assignment of the extinction-to-backscatter ratio of the CALIOP lidar (Campbell et al. 2012).

CHAPTER III

METHODS

Collocation of Data Sets

In order to evaluate multiple remotely sensed data sets, it is necessary to collocate all data in both space and time. The first step of the collocation process is to find all MYD06 MODIS files, which lie within the temporal boundaries of a single OMAERUV OMI file. OMAERUV swath files cover a time span of roughly 54 minutes while MYD06 files are broken up into 5 minute swath files, therefore all MODIS files with a start time within 30 minutes of the start or end time of the single OMI file are identified. The AURA satellite trails the Aqua satellite by roughly 15 minutes therefore choosing 30 minute intervals ensures that all possible data is collocated while limiting the comparison of the data sets to the same overpass from each satellite. Due to the large footprint of OMI pixels, the OMPIXCOR product is utilized in order to establish an area that is representative of the area covered by individual OMI pixels. Next, all MODIS pixels within the boundaries of the current AI pixel are identified and the corresponding OMI AI value is assigned to all collocated MODIS pixels. Note that in the scenario where a single MODIS pixel is paired with more than one OMI pixel, the closest OMI AI value is assigned to the MODIS pixel if the difference in OMI AI between the two neighboring OMI pixels is less than one. In the case where the difference in OMI AI pixels is greater than one, the particular MODIS pixel is not considered collocated.

Next, a similar method described above is used in order to find paired data between the collocated MODIS data set and CALIOP cloud and layer aerosol products L2_05kmCLay and

L2_05kmALay, respectively. The temporal boundaries are retrieved from the original OMI file in order to identify all daytime CALIOP files within 30 minutes of the start or end time. Due to the limited spatial information of the MYD06 files, the 1 km geolocation product, MYD03, files are used in order to assign unique spatial coordinates to all individual MODIS cloud property retrievals. This proved to be necessary in comparing MODIS to a nadir viewing sensor such as CALIOP. Spatially, CALIOP and MODIS observations are considered collocated when the center of a MODIS 1 km x 1 km retrieval is identified within 3 km of the temporal midpoint for a 5km L2_05kmALay profile. Several MODIS observations can be paired with a single CALIOP scene such that all MODIS pixels found to have a collocation with a 5 km CALIOP profile will be assigned the corresponding CALIOP AOD.

Data Filtering

The OMI and MODIS datasets containing global observations on a daily basis are rather large. Thus analyzing and comparing two such data sets can be computationally and temporally expensive. In order to conserve resources and time, several data screening criteria are applied before the collocation process.

The OMAERUV product contains bad AI retrievals also known as fill values, which are removed before performing the collocation process and account for about 25-30 % of the original cloudy OMI data scenes. Only aerosol plumes with AI values greater than 0.5 are considered because small AI values generally indicate a large uncertainty in retrievals (Torres et al. 2007). In order to retain the best viewing conditions, only scenes with a VZA less than 55° and path length defined as $1/\cos(\text{SZA}) + 2/\cos(\text{VZA})$ with values between 3 and 7 are considered similar to Yu et al. 2011. The quality of each OMI AI scene is retrieved from the 'FinalAlgorithmFlags'

parameter. The first 3 bits give information about the reliability of the data while the 6th and 7th bits give information about the viewing geometries. OMI scenes which meet the following criteria are used; most reliable, reliable and least reliable data, the SZA less than 70° and sun glint angle over water greater 40°.

This study is concerned with scenes which are completely opaque and therefore only MODIS scenes with a cloud fraction of one and very good quality data are considered. Recall from the data section that the cloud fraction and its QA flags are directly derived from the MODIS Cloud Mask and its QA flags. Thus, a cloud fraction of unity ensures all 1 km cloud mask scenes are found to be cloudy pixels with very good quality. Different spatial resolutions of the cloud fraction and cloud optical properties called for the use of various different QA parameters to be applied to the MYD06 data set. The ‘Quality Assurance_1km’ parameter contains QA information for all cloud optical properties including COD and r_e for both standard and supplementary MODIS products. Only positive values of good and very good quality standard and supplemental CODs are considered, which limited the study region to over ocean scenes. It should be noted that during the MODIS comparison to the nadir-viewing instrument CALIOP, the lack of unique spatial coordinates for 1 km MODIS products proved to be an issue. Therefore, the MYD03 geolocation file is used in order to retrieve unique geolocation information for each 1 km MODIS scene. Only MYD06 files which have a corresponding MYD03 file are used.

CALIOP cloud and aerosol products (L2_05kmClay and L2_05kmAlay) are used such that: (1) only aerosol files having a corresponding cloud file are used and (2) the cloud product is used to find the presence of low level single layer clouds and therefore, very lenient QA is applied to the cloud product data. In order to find the low level optically thick water clouds, the

cloud top height is restricted to less than 3 km while focusing only on single layer clouds. This ensures that our identified low level cloud top is the same cloud that our passive sensor, MODIS, is detecting.

To derive above-cloud column AOD (τ), the Extinction Coefficient at 0.532 μm (β), defined as the attenuation of light through the aerosol plume due to both absorption and scattering in this part of the spectrum, is integrated through the aerosol plume height found above the low level cloud top height. It is computed using

$$\tau = \int_{z_{cloud-top}}^{z_{TOA}} \beta dz \quad (3)$$

where $z_{cloud-top}$ represents the height of the cloud top and z_{TOA} represents aerosol plume top height. Note that profiles where AOD is solved as zero after CALIOP QA screening are considered invalid and neglected for the study. The ‘Column_Optical_Depth_Aerosols_532’ is the pre-calculated AOD for the entire column while Eq. (3) gives the calculated AOD for all plumes identified above the cloud. In order to ensure that any plumes below the identified cloud are not contributing to the calculated AOD, the CALIOP column is used only if the calculated AOD is equal to the column AOD. Before deriving the calculated AOD, however, L2_05kmALay profiles are subject to QA screening before a solution is reached. An identified layer is considered quality assured and included in the calculated AOD when all of the following criteria are satisfied:

- $-50 < \text{CAD} < -100$
- Feature Flag is equal to 27 or 19

The CAD Score is a measure of the confidence of the classification of a layer as aerosol or cloud within a bin. Negative values of the CAD Score indicate the presence of aerosols (Campbell et al. 2012). For each layer detected in the CALIPSO backscatter data, a set of feature

classification flags is derived which report the feature type (bits 1-3) and feature subtype (bits 4-5) while the remaining bits describe the phase of water/ice and subtype features for identified cloud and aerosol layers. For the purposes of this study, the first 3 bits are used to ensure the detected layer is an aerosol layer and bits 4-5 are used to describe the confidence of the retrieved layer. CALIOP aerosol layer data of high and medium confidence are used similar to Yu et al. 2011.

CHAPTER IV

RESULTS AND DISCUSSIONS

Results from the study are separated into four different sections. First, the wide swaths of passive sensors OMI and MODIS are utilized in order to identify the global distribution of above-cloud aerosols on a daily basis. Second, a case study is carried out over one of the identified regions from the first section in order to determine the impacts above-cloud aerosols may have on individual retrievals. Third, seasonal climatological impacts on cloud property retrievals are discussed over the various identified regions evaluated using only passive sensor retrievals. Lastly, the active remote sensing LIDAR on board CALIOP is incorporated into the study allowing us to gain an understanding of the vertical distribution of clouds and aerosols not explored by the passive sensor study.

Global Distribution

Aerosols originate from natural sources such as desert dust, sea salt, forest fires, sulfate aerosols, and volcanic ash. They can also originate from anthropogenic sources (man-made) such as fossil fuel combustion and biomass burning. Aerosols can also be classified according to their size. Dust and sea salt aerosols are typically coarse mode while pollution and biomass burning aerosols are classified as fine mode aerosols. Particle size is the main factor determining the residence time of aerosols in the atmosphere. Larger aerosols (coarse) typically remain in the atmosphere for a few days while smaller aerosols (fine) can remain in the atmosphere for weeks, months and some instances even years (Brock et al. 1993).

The initial analysis shows the global and seasonal distributions of UV-absorbing aerosol loading (OMI AI) over cloudy MODIS regions as described in the methodology section. Figure 1 is generated using OMI level 2 swath data collocated with MODIS Aqua collection 5 and shows elevated (above-cloud) OMI AI values over cloudy MODIS pixels averaged into a $0.25^\circ \times 0.25^\circ$ grid boxes for 2007 and 2008 combined. Above-cloud aerosol events occur in various locations throughout the globe which varies from season to season. Figure 1a shows a large concentration of above-cloud aerosol over the Saharan desert region in northern Africa, as well as in southeastern Asia off the coast of north Vietnam (Gulf of Tonkin) during the boreal spring (March, April, May or MAM) which is the typical season for East Asian dust storms. The spring and summer oceanic transport of dust across the Atlantic Ocean and spring transport of Asian dust across the Pacific Ocean to North America are well documented using satellite observations (Kaufman et al. 2005). Large above-cloud aerosol loading can also be seen in Northern China's desert region. However, this region is not a focus region due to the limitations of the MODIS supplementary retrievals (refer to data section). Most of the above-cloud aerosols over the Gulf of Tonkin originate from Northern Vietnam and are largely a result of the drastic increase in population over the past 20 years in Northern Vietnam (Bac and Hien, 2009). The aerosols over the Gulf of Tonkin vary in origin from long range transport aerosols, industrial aerosols from coal fired plants and vehicles, marine aerosols and biomass burning. A clear difference can be seen in the aerosol concentration between the northern and southern hemisphere during the spring dust storms.

Large amounts of above-cloud absorbing aerosol loading can be seen in Figure 1b, with a seasonally averaged OMI AI as high as 3.0, over the smoke outflow region (Latitude: 22°S - 5°N and Longitude 18°W - 15°E) off the western coast of Angola during the summer months (June,

July and August or JJA). Large dust outbreaks, during this season, appear to be associated with strong convective disturbances that develop in Western Africa and move westward (Prospero et al. 1996). As they move over the ocean, the dust events are usually associated with easterly waves which emerge from the west coast of Africa every 3-4 days and transport the dust across the Atlantic Ocean to the Caribbean in about a week (Ott et al. 1991), visible in figure 1b. The southwest coast of Africa has consistently been identified as the world's largest single source of biomass burning due to farmers setting fires to rainforests in order to clear land for agricultural purposes (Roberts et al. 2008) also visible in Figure 1b. The biomass burning aerosols measured by AERONET in Zambia during the savanna-burning season were found to have the largest absorption (lowest SSA) ever measured at any AERONET site (Dubovik et al. 2002; Giles et al. 2012) making this region the focal point of our case study in the proceeding section.

The frequency of absorbing aerosols over cloudy scenes is also checked during this study. Figure 1c shows the frequency of above-cloud absorbing aerosol pixels (defined as the ratio of cloudy OMI pixels with AI greater than 1 to all cloudy OMI AI pixels) during the northern hemisphere spring for 2007 and 2008. Only pairs of MODIS and OMI data that have valid OMI AI values, with 100% cloud coverage as reported by the collocated MODIS cloud products are shown. Above-cloud aerosol scenes are rare in the dust outflow region during the seasonal spring (~30%) as opposed to the summer months which may be attributed to the lack of clouds over dry and arid desert regions during the spring months. The Gulf of Tonkin also experiences higher percentages of above-cloud aerosol pixels (~30%) during the seasonal spring, as can be seen from the Figure 1c, with absorbing aerosols originating from several different sources ranging from anthropogenic bio-mass and industrial pollutants.

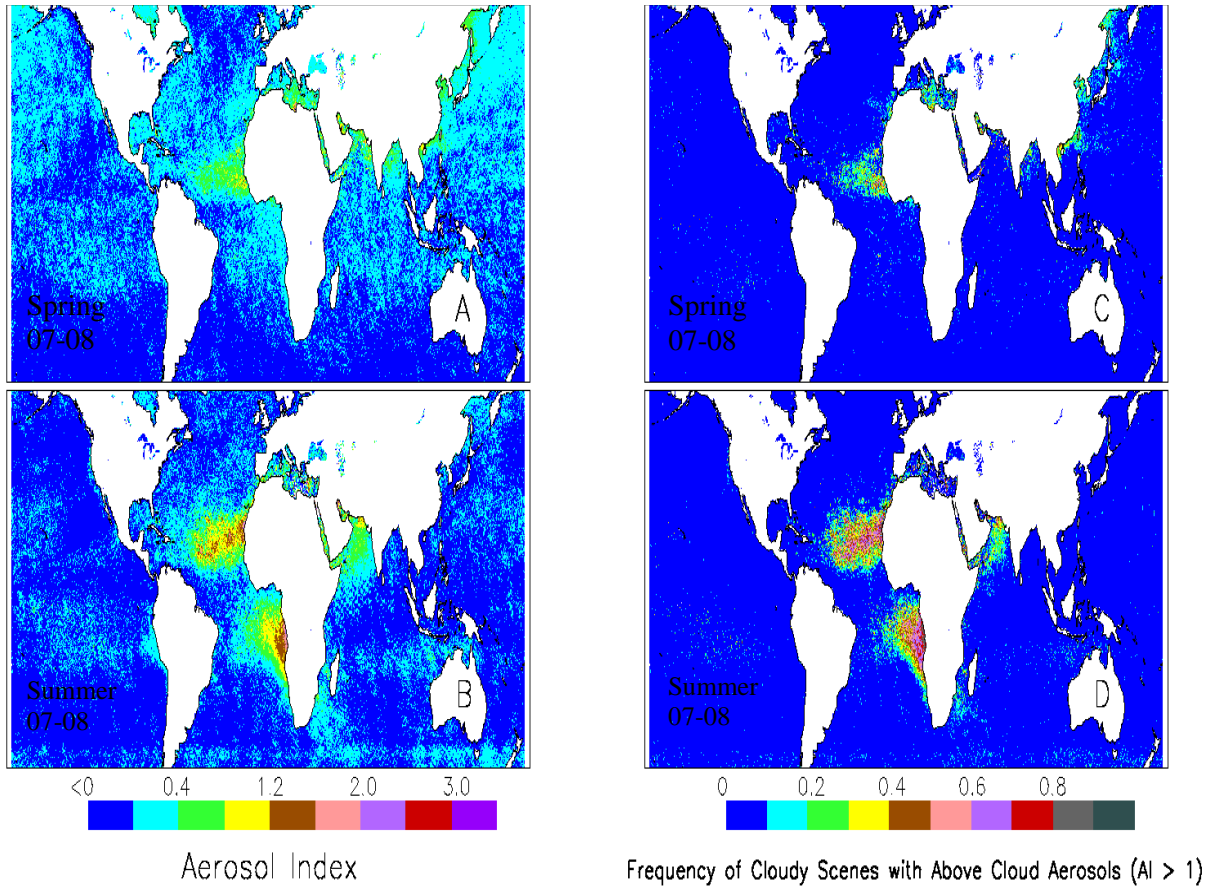


Figure 1. Two year (2007-2008) spatial plot (a) seasonal Ozone Monitoring Instrument (OMI) Aerosol Index (AI) over cloudy scenes during the summer season (June, July, August or JJA) for 2007 and 2008 combined, (b) The seasonal OMI AI average over Moderate Resolution Imaging Spectroradiometer (MODIS) cloudy scenes during the spring season (March, April, May or MAM) for 2007 and 2008, (c) frequency of occurrence of above-cloud aerosols ($AI > 1$) for the summer of 2007 and 2008, (d) same as 1c for the JJA of 2007-2008.

While over most of the oceans, the frequency of occurrence is close to 0, a significant percentage of the frequency of occurrence ($> 50\%$) is found over both the smoke and dust outflow regions during the boreal summer as seen in figure 1d. It should be noted that the frequency occurrence from Figs. 1c-d may be overestimated, as some observed scenes could have valid cloudy MODIS retrievals however with invalid OMI AI values. Such scenes are filtered out before the collocation process as described previously in the methods section.

Case Study

Figure 2 shows the example of an above-cloud aerosol scenario over the west coast of South Africa for 04 August 2007 at 1300 UTC. The true color image of an aerosol plume lifted above the stratocumulus cloud deck is evidenced by darkening of the cloudy region. For the same region, the OMI AI plot shows the OMI AI values could reach up to 4 indicating the presence of a heavy aerosol plume above clouds. This region as shown in Figure 1 is known as the “smoke outflow” region during the summer (Yu et al. 2011). The cloud top temperature of the stratocumulus cloud deck is around 280-290 K showing that the stratocumulus cloud deck is indeed a low level water cloud. The CALIOP 0.532 μm vertical backscatter profile confirms the presence of a low-level cloud at about 1 km with a smoke aerosol plume which extends from 2-5 km in altitude for the smoke outflow region (CALIOP overpass is also shown in the MODIS true color image as the red line). The cloud optical depth retrievals from the standard (visible), labeled as visible τ in figure 2, and the supplementary shortwave infrared MODIS cloud products, labeled as the shortwave infrared τ are also shown. These data are created by averaging pairs of valid retrievals from both the standard and supplementary MODIS cloud products at 1 km resolution into 5 km aggregates. Although the general patterns are similar, the differences are clearly observable. The difference in COD ($\Delta\tau$) between each pair of 5 km the standard and supplementary products can also be seen in figure 2. While comparing with the OMI AI plot (Fig. 2b) in addition to neglecting the noisy data points, the ΔCOD patterns match the OMI AI patterns over the regions with OMI AI values larger than 2 (AOD \sim 0.1-0.3 for smoke aerosols, AOD \sim 0.3-0.5 for dust aerosols, Yu et al. 2012). The COD values from the shortwave infrared method are less sensitive to the presence of fine mode aerosols such as biomass burning aerosols whereas the visible COD retrievals are subject to above-cloud absorbing smoke aerosol

contamination and consequently causing the ΔCOD pattern to correlate well with the OMI AI pattern. Figure 2 suggests that a reduction of COD value of 2-5, against an average COD value of ~ 10 , could exist using the visible COD retrieval method for regions that have above-cloud smoke plumes with OMI AI values of 2-4. MODIS r_e retrievals from the standard and supplementary MODIS r_e data are shown in the figures labeled visible r_e and shortwave infrared r_e , respectively, in units of microns. Unlike the COD retrievals, no apparent correlation is found between OMI AI and the difference in r_e values between the two MODIS r_e datasets, Δr_e , suggesting that above-cloud aerosols may have an insignificant effect to the r_e retrievals. Therefore, we focus our discussions solely on COD.

Seasonal and Regional Impacts

Passive Remote Sensing

The impacts on MODIS visible COD retrievals are evaluated for some of the previously identified regions including the northwestern coast of Africa during the spring and summer seasons, the Gulf of Tonkin coast during the East Asian spring dust storms, and the southwestern coast of Africa during the Northern Hemisphere Summer.

Using collocated OMI AI and MODIS COD products, the difference in visible and shortwave infrared COD retrievals (ΔCOD from MODIS) is examined in the presence of high OMI AI values off the southwestern coast of Africa, also known as the smoke outflow region (Yu et al. 2011), during the Northern Hemisphere Summer. Results for the smoke outflow region (Latitude: 22°S - 5°N and Longitude: 18°W - 15°E) are shown in Figure 3 below.

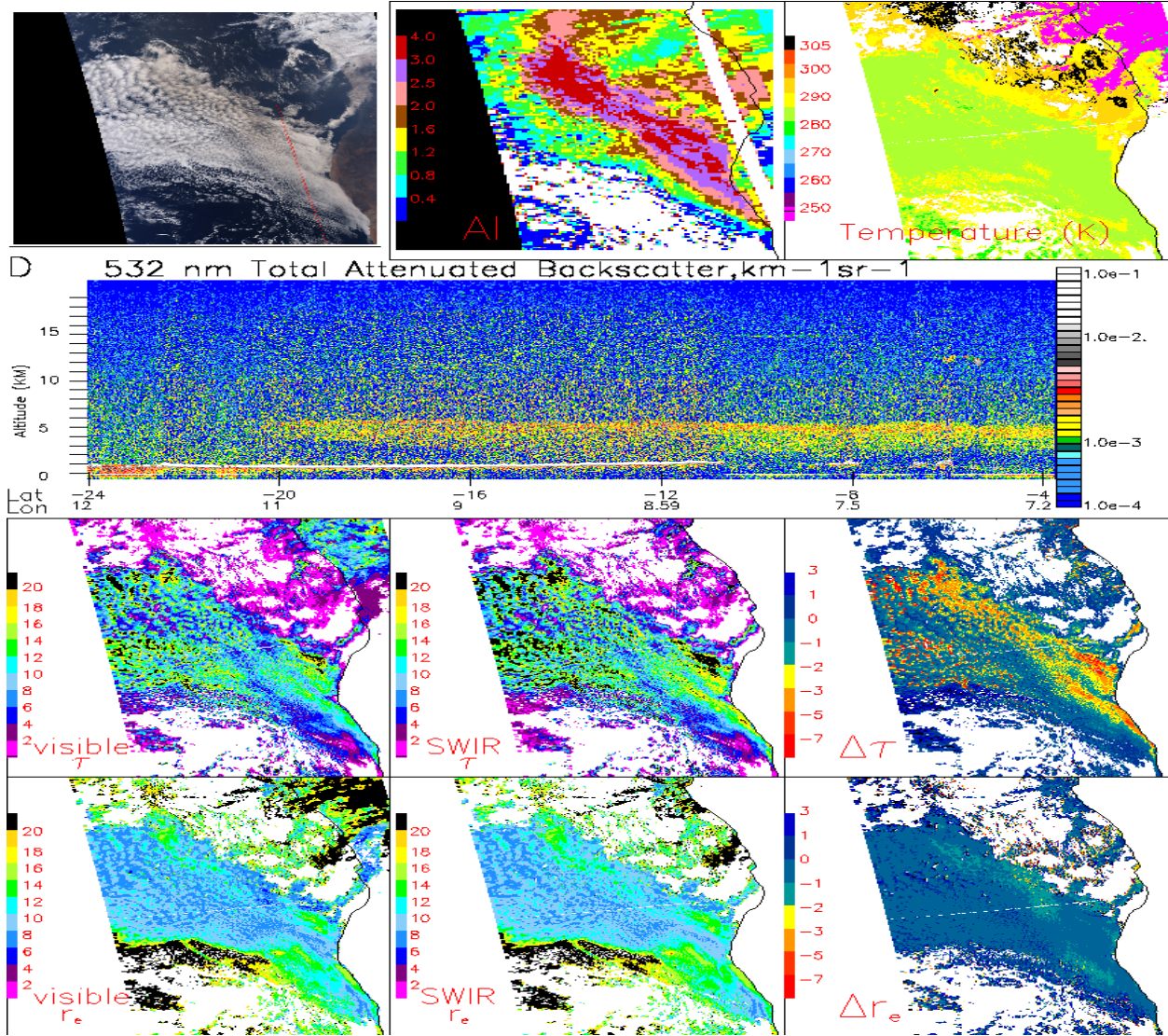


Figure 2. Case study of collocated Ozone Monitoring Instrument (OMI) and Aqua Moderate Resolution Imaging Spectroradiometer (MODIS) on August 4th, 2007 at 13:00 UTC. Top left corner shows the MODIS true color image off the southwest coast of Africa. The red line visible in the image is the Cloud-Aerosol Lidar with Orthogonal Polarization (CALIOP) overpass. The top middle diagram depicts the Ozone Monitoring Instrument Aerosol Index (OMI AI), retrieved from collocated MODIS data set, for the same area as the MODIS true color image. Top right figure corner figure shows the cloud top temperature from MODIS for the same area as MODIS true color image. The vertical CALIOP backscatter can be seen, figure in second row, confirming the presence of an aerosol plume suspended over a low level cloud. Figure in the third two to the left shows the cloud optical depth (COD) using the standard MODIS COD data aggregated into a 5 km product. Middle plot on the third row shows the COD retrieval using the supplementary MODIS COD data. Right figure on third row shows the difference in COD retrievals (standard vs. supplementary) using only valid pairs of COD data. The last row shows the standard effective radius retrievals, supplementary retrievals and difference in retrievals, respectively, similar to COD in units of microns.

Figure 3a shows the averaged MODIS Δ COD as a function of OMI AI for every 0.1 OMI AI bin. In order to exclude ice clouds, only COD retrievals with cloud top temperatures above 275 K are used. The MODIS Δ COD and OMI AI relationship is also evaluated based on five COD ranges: 0-4, 4-8, 8-12, 12-16 and 16-20. To exclude noisy data, we have also implemented a two standard deviation data trim where only data points within 2 standard deviations of the mean are used in the averaging process. With the exception of the 0-4 COD range, all other COD ranges demonstrated a decrease in MODIS Δ COD as the OMI AI values increase, while the larger the COD, the larger the negative value of MODIS Δ COD. For example, an average decrease in MODIS Δ COD of 2 is found when OMI AI value approaches 3, for the COD range of 8-12. For the COD range of 16-20, the averaged MODIS Δ COD of 4 is found when OMI AI value approaches 3. Given that the stratocumulus cloud deck over the study region is not optically thick (e.g., COD \sim 10 as shown in Fig. 1), the uncertainties in MODIS COD from the standard product could be significant over this region and need to be accounted for. To double check the results, we have repeated the exercise using the collocated MODIS and OMI data for the northern hemispheric summer of 2008 (Fig. 3c). Results found from the 2008 data are consistent with our findings from 2007.

We have also studied the MODIS Δ COD and OMI AI relationship (Figs. 3b and 3d) over the northwest coast of Africa (Latitude: 5°N - 30°N and Longitude: 60°W - 16°W) which is known as the “dust outflow” region (Yu et al. 2011) during the Northern Hemisphere Summer. Similar to our smoke aerosol studies, we have evaluated this relationship as a function of COD. No observable decrease in MODIS Δ COD is found as the OMI AI increases for the above-cloud dust cases. Similar findings are found for using data from both the summer of 2007 and 2008. The results are not surprising as dust aerosols have a much larger particle size (\sim 1 μ m) in

comparison to smoke aerosols (sub-micron). However, unlike smoke aerosols, the above cloud dust plumes could impact COD retrievals at both the visible and the shortwave infrared spectrum. Other methods are needed to evaluate the impacts of above-cloud dust aerosols to the MODIS COD retrievals.

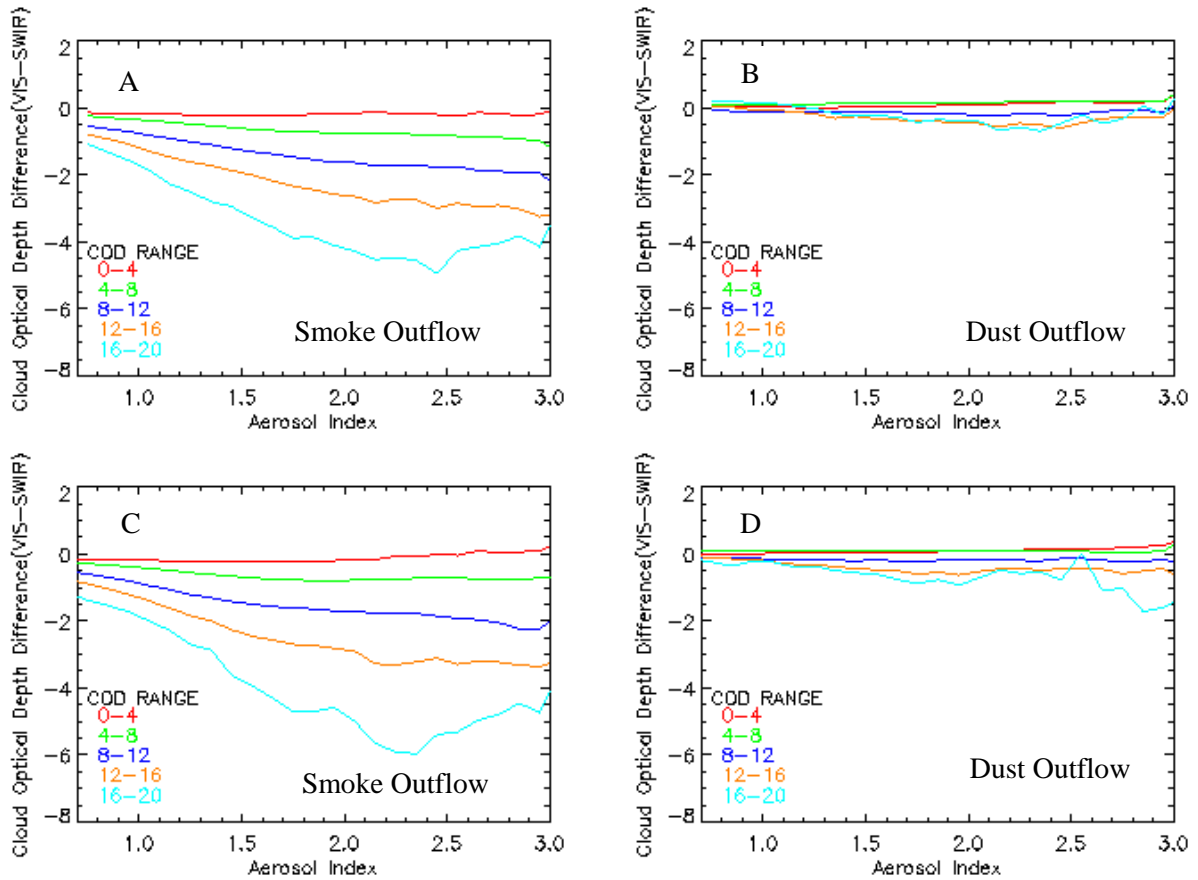


Figure 3. Scatter plot of Ozone Monitoring Instrument (OMI) Aerosol Index (AI) vs. binned averaged difference between retrieved standard and supplementary cloud optical depth (Δ COD) from Moderate Imaging Resolution (MODIS) as a function of COD (a) for the ‘smoke outflow’ region (22° S - 5° N and 18° W - 15° E) for June-August, 2007, (b) for the ‘dust outflow’ region (5° N - 30° N and 60° W - 16° W) during June-August, 2007, (c) for the ‘smoke outflow’ region of June-August 2008 and (d) for the ‘dust outflow’ region for June-August 2008.

Following Eck et al. (2013), we studied the ΔCOD and OMI AI relationship for two seasons, July-August (solid line) and September-October (dotted line) for 2007, over the smoke outflow region (Fig. 4a). Higher SSA values are associated with biomass burning aerosols during later bio-mass burning months of September and October. The lower absorption of the smoke aerosol plume may be attributed to several factors such as possible differences in fuel types (different vegetation being burned) and differences in transport time from the different burning regions (Eck et al. 2013). Lower ΔCOD values, on the order of 0.5 at the OMI AI values of 2.0, are found during the latter part of the year (September –October) compared to the middle part of the summer biomass burning season (July-August), which is attributed to the higher SSA values later in the season. The higher SSA values (lower absorption) reduces the biases on the COD retrievals associated with above-cloud smoke aerosols as can be seen from Figure 4a. We have repeated the exercise for the year of 2008. Figure 4b does not show a similar trend as the 2007 biomass season which can be attributed to the annual variation of the southern Africa aerosol SSA.

The Gulf of Tonkin also sees high aerosol concentrations from local sources such as soil, re-suspended road dust, coal fly ash and biomass burning which can be transported eastward atop cloud decks during the early spring months (Bac and Hien, 2009). A similar analysis is carried out over this region (Latitude: 17°N - 25°N and Longitude: 105°E - 120°E) (Figure 5). Data are trimmed similar to Figure 3 while limiting the data to cloud top temperatures above 275 K and binning the data into five different COD groups. Figure 5a shows the relationship between OMI AI and ΔCOD for the early spring of 2007. A clear relationship can be seen between $\Delta\text{MODIS COD}$ and OMI AI over the Gulf of Tonkin region similar to the smoke outflow region in southern Africa. Figure 5b shows the same relation for the 2008 spring season.

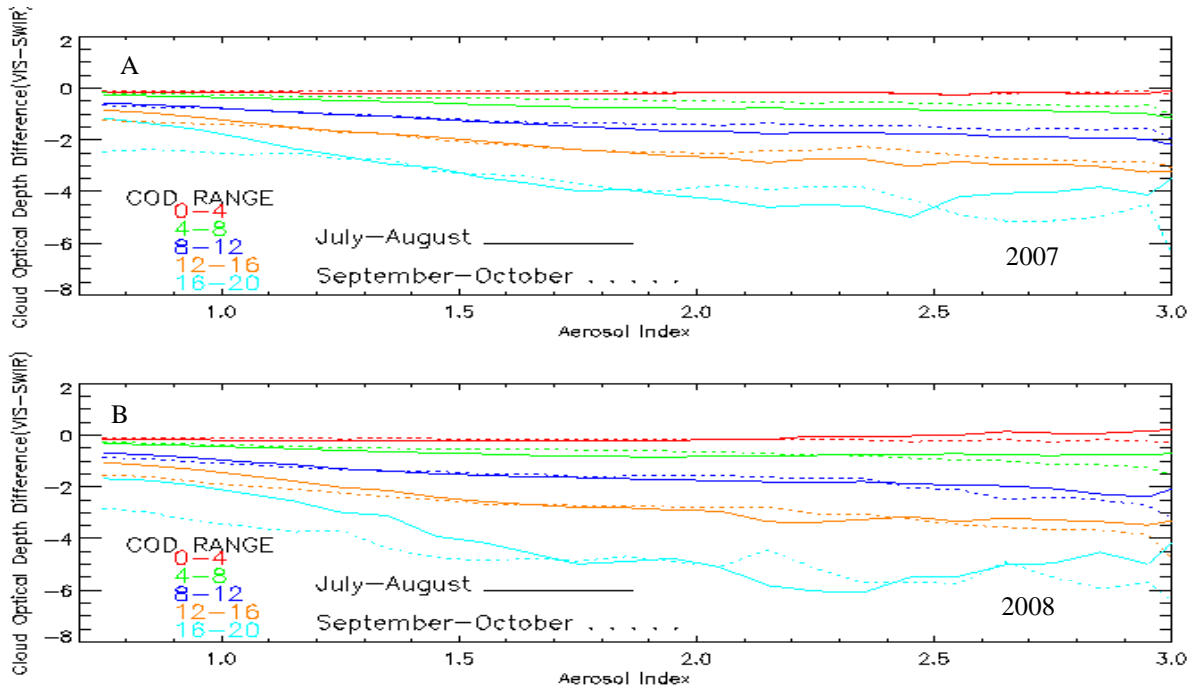


Figure 4. Scatter plot of Ozone Monitoring Instrument (OMI) Aerosol Index (AI) vs. binned averaged difference between retrieved standard and supplementary cloud optical depth (ΔCOD) from Moderate Imaging Resolution (MODIS) as a function of COD separated into early months of the biomass burning season July and August – solid line) and later burning months (September and October dotted line) over ‘smoke outflow’ region ($22^\circ\text{S} - 5^\circ\text{N}$ and $18^\circ\text{W} - 15^\circ\text{E}$) during the (a) the 2007 biomass burning season and (b) during the 2008 biomass burning season.

Active Remote Sensing

As shown from previous studies (Yu et al. 2011), above-cloud OMI AI is also a function of underlying COD. Therefore, another experiment is conducted, utilizing one year of data (2007), in order to establish a relationship between OMI AI and above-cloud CALIOP AOD similar to Yu et al. (2011). Figure 6 below shows the relationship between OMI AI and CALIOP AOD as a function of the underlying COD for the smoke and dust outflow region described previously. Similar to before, the cloud layer product is used to locate low-level single layer clouds while the aerosol layer product is used to calculate the above-cloud AOD. Higher

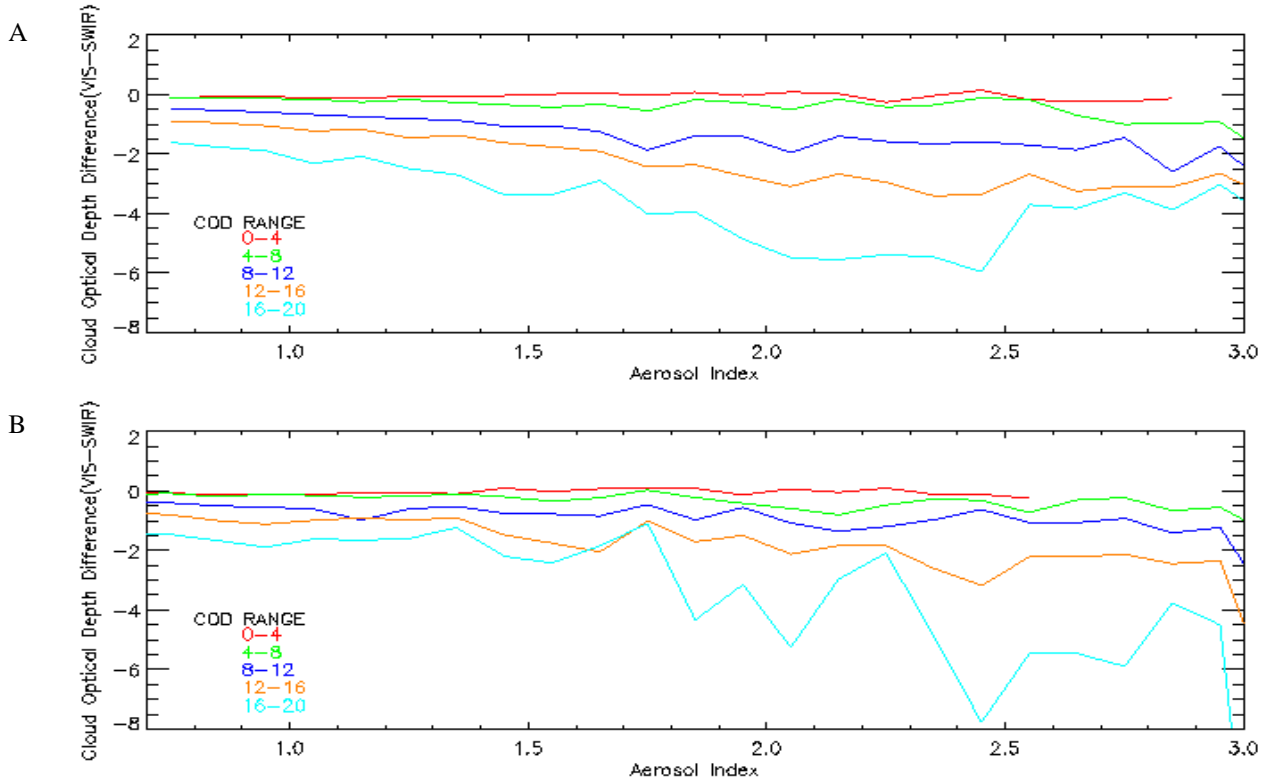


Figure 5. Scatter plot of Ozone Monitoring Instrument (OMI) Aerosol Index (AI) vs. binned averaged difference retrieved standard and supplementary cloud optical depth (Δ COD) from Moderate Resolution Imaging Spectroradiometer (MODIS) for the Gulf of Tonkin region off the coast of Northern Vietnam (7°N - 25°N and 105°E - 120°E) during the early spring dust storms months (February, March, April or FMA) for (a) 2007 and (b) 2008

OMI AI values are associated with any particular CALIOP AOD in the smoke outflow region (Figure 6a) when compared to the dust outflow region (Figure 6b) due to the higher absorption of the smoke aerosols.

We further evaluate the effects of above-cloud aerosol to COD retrievals using collocated CALIOP AOD and MODIS COD data. Figure 7a shows the relationships between the above-cloud CALIOP AOD and MODIS Δ COD as a function of COD during the 2007 summer season in the smoke outflow region. Similar to Figure 3, cloud top temperatures are restricted to 275 K and above. Also similar to Figure 3, a two standard deviation data trim is applied. Decreases in

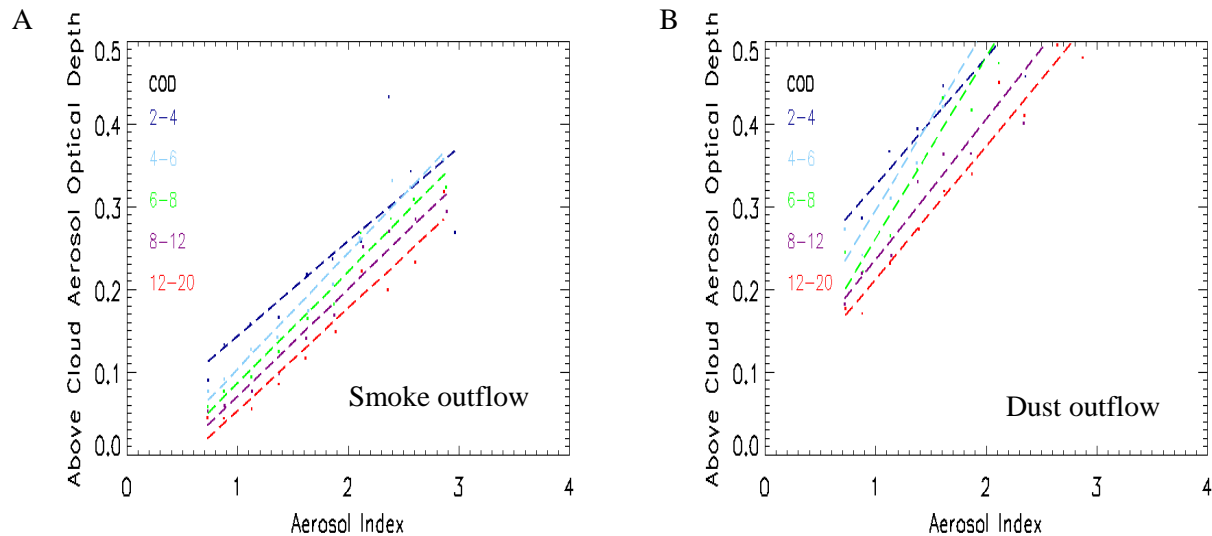


Figure 6. Scatter plot of Ozone Monitoring Instrument (OMI) Aerosol Index (AI) vs. Cloud-Aerosol Lidar with Orthogonal Polarization (CALIOP) above-cloud AOD from CALIOP a function of the underlying Moderate Resolution Imaging Spectroradiometer (MODIS) COD during the summer of 2007. The AI are binned into 0.1 increments while the AOD is binned into 0.01 increments and the COD as shown in plot is binned into for (a) the smoke outflow region and (b) for the dust outflow region.

MODIS Δ COD are found for COD > 4, and the larger the COD value is, the stronger the decrease in MODIS Δ COD. Note for the near zero CALIOP AOD case, the higher the MODIS COD is, the lower the negative MODIS Δ COD. For example, for the near zero CALIOP AOD bin, a near zero MODIS Δ COD is observed for COD of 0-4 and a -2 MODIS Δ COD is observed for the COD range of 16-20. We are unsure whether this phenomenon is caused by issues related to MODIS COD retrievals or simply because the above-cloud CALIOP AOD is also sensitive to COD. We leave this problem for a future study as well.

Note that the collocated MODIS, OMI and CALIOP dataset is much smaller in size in comparing with the collocated MODIS and OMI dataset. It is necessary to ensure that the OMI AI and MODIS COD relationship suggested from Figure 3 is still valid for the MODIS, OMI and CALIOP dataset, so as to justify the validity of Figure 7a. For this purpose, we also recomputed

the relationships between OMI AI and MODIS Δ COD as a function of COD using only pairs of collocated MODIS and OMI data that are consistent with the collocated CALIOP and MODIS data used in creating Figure 7a. Results shown in Figure 7b are similar to what is presented in Fig. 3. The same procedure is carried out for the dust outflow region and again, no significant relation is found between above-cloud CALIOP AOD and Δ COD (Fig. 7c). It should be noted that the last COD range is not shown in Fig. 7c due to the limited number of samples and high amounts of noise.

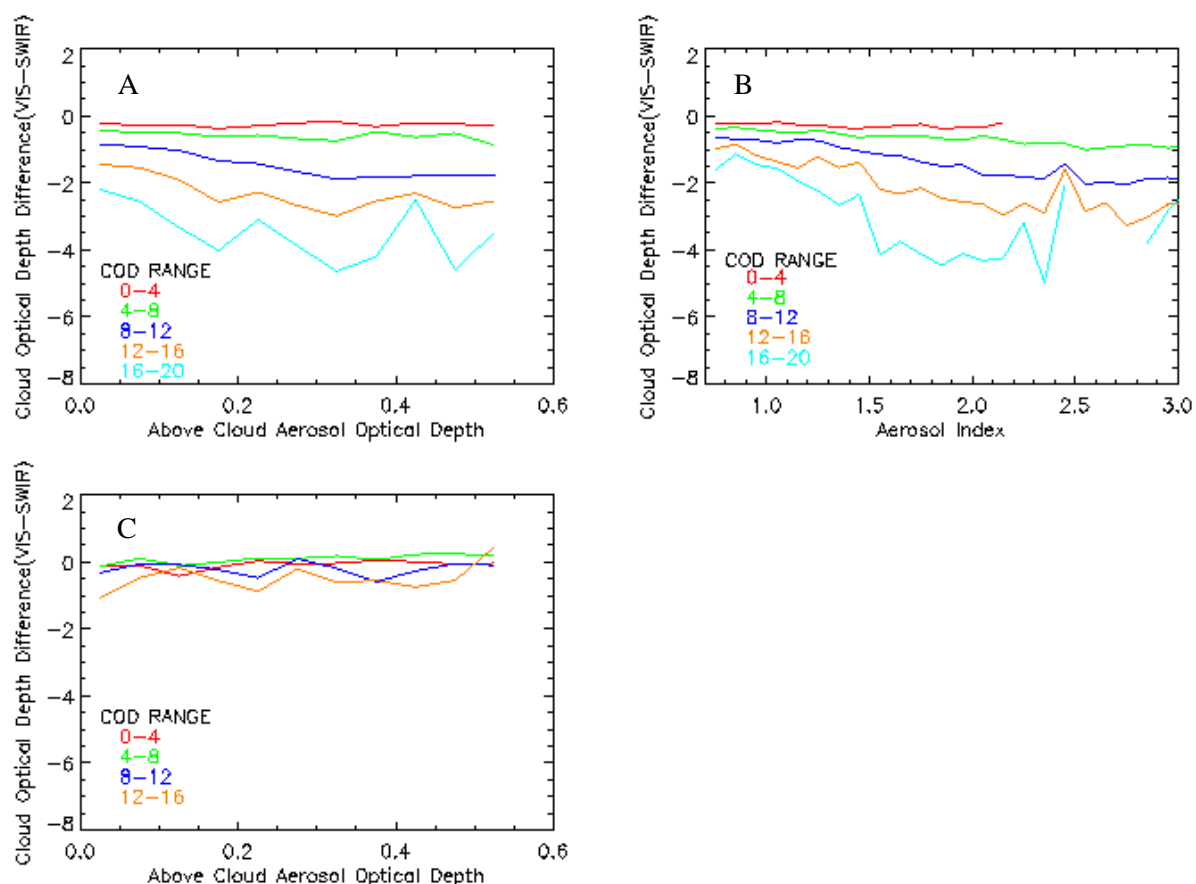


Figure 7. Figure 7a shows the relationship between cloud CALIOP AOD and Δ COD in the smoke outflow region during the 2007 summer. Figure 7b shows the relation between OMI AI and Δ COD only over CALIOP overpasses that are used for creating Figure 7a. Figure 7c shows the above-cloud aerosol loading (CALIOP AOD) and Δ COD for the dust outflow region during the summer of 2007. The cod range of 16-20 is removed from figure 7c due to limited number of collocated CALIOP pixels and high amounts of noise.

Like most studies, this study has its limitations as far as scene type, aerosol type and size and cloud height and phase. For starters the OMI algorithm infers, as opposed to detects, the presence of aerosols from their absorption. Therefore, only aerosols which absorb in the near UV spectrum can be used in this study which includes bio-mass burning and desert dust aerosols. Absorbing aerosols which are mixed in with the cloud layer cannot be detected therefore only aerosols which are lofted above clouds are used. The MODIS cloud detection algorithm uses a cirrus cloud filter and also contains a cloud top temperature parameter allowing us to focus in on low-level optically thick water clouds. With the aid of the lidar on-board CALIOP, we are able to focus on single layer low-level optically thick water clouds at nadir of our passive sensor swaths. The standard and supplementary cloud top property retrievals from MODIS allow us to locate biases on COD retrievals associated with smoke aerosols however the larger dust aerosols are not transparent to the longer wavelength supplementary retrievals, therefore the study is limited to sub-micron sized smoke aerosols. Lastly, the study is restricted to over ocean scenes due to the supplementary product's inability to retrieve over land.

CHAPTER V

SUMMARY AND CONCLUSION

This thesis analyzes the frequency distributions as well as the impacts of above-cloud aerosols to the standard Moderate Resolution Imaging Spectroradiometer (MODIS) cloud optical depth (COD) data, using visible and shortwave-infrared MODIS cloud optical depth (COD) retrievals from NASA Collection 5 Aqua MODIS (1 km x 1 km spatial resolution, 0.86 μm (standard) and 1.60 μm (supplementary)) collocated with Ozone Monitoring Instrument (OMI) and Version 3.01 Cloud-Aerosol Lidar with Orthogonal Polarization (CALIOP; 5 km along-track average, 0.532 μm) datasets over most of the globe. Accurate MODIS cloud property retrievals are important since passive satellite sensor retrievals can serve as a basis for cloud climatological studies (Haywood et al. 2004; Platnick et al. 2003). Standard and supplementary cloud property retrievals are compared in the presence of above-cloud aerosols retrieved from passive (OMI Aerosol Index, AI) and active (CALIOP Aerosol Optical Depth, AOD) satellite-based sensors.

MODIS COD and OMI AI are analyzed in order to locate the sources and track the transportation of above-cloud aerosols throughout the globe on a daily basis. This study shows various sources of absorbing aerosol lofted atop low-level clouds throughout the year (Figure 1). A case study is conducted off the southwest coast of Africa for a smoke layer lofted atop a stratocumulus cloud deck that illustrates a bias on visible MODIS COD retrievals in the presence of high OMI AI values. The climatological study over a two year period (2007-2008) suggests that above-cloud smoke aerosols, which occur more than 50% of the time, create up to a 20% uncertainty in the MODIS visible COD in the smoke outflow region in southern Africa during

the boreal summer. This uncertainty is a function of the smoke single scattering albedo (SSA) particularly during the Northern Hemisphere Summer. The COD retrievals from a consistent cloud deck over Vietnam's Gulf of Tonkin region during the early spring also show a bias, similar in magnitude to the southern Africa cloud deck. A similar analysis is also conducted over the dust outflow region in northern Africa, however, no significant relationship is found between OMI AI and MODIS ΔCOD . This may be due to possible dust aerosol influences on MODIS COD retrievals in both the visible and the shortwave infrared spectrum. The impact of above-cloud aerosol smoke and dust aerosols on standard MODIS r_e retrievals is also examined and no significant relationship is found between OMI AI and MODIS Δr_e . Future studies utilizing cloud property retrievals taken at longer wavelengths may be needed in order to investigate the impact dust aerosols may have on the underlying cloud COD and/or r_e .

The use of OMI AI values is only semi-quantitative, as optically reflective clouds may raise the value of OMI AI without actually increasing the aerosol loading (Torres et al. 1998). However, a fairly linear relationship has been found between the above-cloud OMI AI and above-cloud AOD retrieved from CALIOP on board the Cloud-Aerosol Lidar and Infrared Pathfinder (CALIPSO) as a function of COD (Yu et al., 2011). Therefore, measurements utilizing the active sensor CALIOP are used to validate the results from the passive sensor study in both regions. The OMI AI shows a large dependency on the SSA of the aerosols which was found to have a seasonal trend during the biomass burning months. The relationship between OMI AI and MODIS ΔCOD is compared from early to late months of the biomass-burning season in order to ensure the OMI AI can compensate for the change in SSA throughout the course of the biomass burning season. This study also suggests that over the southwest coast of Africa during the boreal summer and fall, both the individual COD retrievals and the

climatological values of the standard MODIS COD could be affected by above-cloud aerosol smoke aerosols. The OMI AI could be used as a means to reduce the uncertainties in the standard MODIS COD data during above-cloud smoke aerosol events.

APPENDIX

APPENDIX A

Acronyms and Definitions

Acronym	Definition
AERONET	Aerosol Robotic Network
AOD	Aerosol Optical Depth
AI	Aerosol Index
AMSR-E	Advanced Microwave Scanning Radiometer - Earth Observing System
CALIOP	Cloud-Aerosol Lidar with Orthogonal Polarization
CALIPSO	Cloud-Aerosol Lidar and Infrared Pathfinder Satellite Observations
EM	Electro Magnetic
GCM	Global Circulation Model
COD	Cloud Optical Depth
GOME	Global Ozone Monitoring Instrument
HERA	Hybrid Extinction Retrieval Algorithm
IR	Infrared
LIDAR	Light Detecting and Ranging
LUT	Look up Table
LWP	Liquid Water Path
MISR	Multi-Angle Imaging Spectroradiometer
MODIS	Moderate Resolution Imaging SpectroRadiometer
NAAPS	U.S. Naval Aerosol Analysis and Predictive System
OMI	Ozone Monitoring Instrument
QA	Quality Assurance
RADAR	Radio Detecting and Ranging
RTM	Radiative Transfer Model
r_e	Effective Radius
SAFARI	Southern African Regional Science Initiative
SCA	Scene Classification Algorithm
SCIAMACHY	Scanning Imaging Absorption spectrometer for Atmospheric Cartography
SHADE	Saharan Dust Experiment
SSA	Single Scattering Albedo
SSR	Solar Spectral Flux Radiance
SWIR	Short Wave Infrared
SZA	Solar Zenith Angle
TOA	Top of the Atmosphere
TOMS	Total Ozone Mapping Spectrometer
UV	Ultra Violet
VFM	Vertical Feature Mask
VZA	Viewing Zenith Angle

References

- Abel, S.J., J.H. Highwood, J.M. Haywood & M.A. Stringer, 2005: The direct radiative effect of biomass burning aerosols over southern Africa *Atmospheric Chemistry and Physics*, 5, 1999-2018.
- Ackerman, S., R. Frey, K. Strabala, Y. Liu, L. Gumley, B. Baum and P. Menzel, 2010: Discriminating clear-sky from cloud with MODIS algorithm theoretical basis document (MOD35), version 6.1. MODIS cloud mask team. Cooperative Institute for Meteorological Satellite Studies, University of Wisconsin-Madison
- Bac, V.T. and P.D. Hien, 2011: Regional and local emissions in red river delta, northern Vietnam. *Air Quality, Atmosphere and Health*, September 2009, volume 2, issue 3, pp 157-167
- Brock, C.A., H.H. Jonsson, J.C. Wilson, J.E. Fye, D. Baumgardner, S. Bormann, M.C. Pitts, M.T. Osborn, R.J. DeCoursey, and D.C. Woods, 1993: Relationships between optical extinction, backscatter and aerosol surface and volume in the stratosphere following the eruption of Mt. Pinatubo. *Geophys. Res. Lett.*, 20, 2555-2558
- Campbell J.R., J.L. Tackett, J.S. Reid, J. Zhang, C.A. Curtis, E.J. Hyer, W.R. Sessions, D.L. Westphal, J.M. Prospero, E.J. Welton, A.H. Omar, M.A. Vaughan and D.M. Winker, 2012: Evaluating nighttime CALIOP 0.532 μm aerosol optical depth and extinction coefficient retrievals. *Atmos. Meas. Tech. Discuss*, 5, 2747-2794

- Chand, D., R. Wood, T.L. Anderson, S.K. Satheesh & J.R. Charlson, 2009: Satellite derived direct radiative effect of aerosols dependent on cloud cover. *Nature Geoscience*, 2, 181-184, doi:10.1038/ngeo437.
- Climate Change 2007 – The physical science basis contribution of working group I to the fourth assessment report of the IPCC (ISBN 978 0521)
- Dubovik, O, B.N. Holben, T.F. Eck, A. Smirnov, Y.J. Kaufman, M.D. King, D. Tanre, and I. Slutsker, 2002: Variability of absorption and optical properties of key aerosol types observed in worldwide locations. *J. Atmos. Sci.*, 59, 590-608.
- Eck, T.F., B.N. Holben, J.S. Reid, M.M. Mukelabai, S.J. Piketh, O. Torres, H.T. Jethva, E.J. Hyer, D.E. Ward, O. Dubovik, A. Sinyuk, J.S. Schafer, D.M. Giles, M. Sorokin, A. Smirnov, I. Slutsker, 2013: A seasonal trend of single scattering albedo in southern African biomass-burning particles: Implications for satellite products and estimates of emissions of the world's largest biomass-burning source. *Journal of Geophys. Res.:Atmospheres*, Vol.118, 6414-6432, doi:10.1002/jgrd.50500, 2013
- Giles, D.M., B.N. Holben, T.F. Eck, A. Sinyuk, A. Smirnov, I. Slutsker, R.R. Dickerson, A.M. Thompson, and J.S. Schafer, 2012: An analysis of AERONET aerosol absorption properties and classifications representative of aerosol source regions. *J. Geophys. Res.*, 117, D17203, doi:10.1029/2012JD018127
- Gladkova, I., M. Grossberg, G. Bonev, F. Shahriar, 2013: A multiband statistical restoration of the Aqua MODIS 1.6 micron band, *Proc. SPIE 8048, Algorithms and technologies for multispectral, hyperspectral and ultraspectral imagery XVII*, 8048819 (May 20, 2011); doi:10.1117/12.883439.

- Hao, W. M., and M.H. Liu, 1994: Spatial and temporal distribution of tropical biomass burning. *Global Biogeochem. Cycles*, 8,495–503.
- Haywood, J. M., S.R. Osborne & J.S. Abel, 2004: The effect of overlying absorbing aerosol layers on remote sensing retrievals of cloud effective radius and cloud optical depth. *Quarterly Journal of the Royal Meteorological Society*, 130, 779–800.
- Herman, J.R., E. Celarier, 1997: Earth surface reflectivity climatology at 340 and 380 nm from TOMS data. *J. Geophys. Res.* 102, 28,003e28,011.
- Hu, Y.-X., D. Winker, P. Yang, B. Baum, L. Poole and L.Vann, 2001: Identification of cloud phase from PICASSO-CENA lidar depolarization: A multiple scattering sensitivity study. *J. Quant. Spectros. Radiat. Tran.*, 70,569-579,2001
- Kato, S., and A. Marshak, 2009: Solar zenith angle and viewing geometry-dependent errors in satellite retrieved cloud optical thickness: Marine stratocumulus case. *J. Geophys. Res.*, 114,D011202, doi:10.1029/2008JDD010579.
- Kaufman, Y.J, and R.S. Fraser, 1997: The Effect of smoke particles on clouds and climate forcing. *Science* 12 September 1997: Vol.277, no.5322, pp.1636-1639.
doi:10.1126/science.27705332.1636
- Kaufman, Y.J, D. Tanre, and Boucher, 2002: A satellite view of the aerosols in the climate system. *Nature* |Vol419|12 September 2002|
- Kaufman, Y. J., I. Koren, L. A. Remer, D. Tanre, P. Ginoux, and S. Fan, 2005: Dust transport and deposition observed from the Terra-Moderate Resolution Imaging Spectroradiometer (MODIS) spacecraft over the Atlantic Ocean. *J. Geophys. Res.*, 110, D10S12, doi:10.1029/2003JD004436.

- Keil, A., and J. M. Haywood, 2000: Solar radiative forcing by biomass burning aerosol particles during SAFARI 2000: A case study based on measured aerosol and cloud properties. *J. Geophys. Res.*, 108, 8467, doi:10.1029/2002JD002315.
- King, M.D., S.C. Tsay, S.E. Platnick, W. Menghua, K.N. Liou, 1997: Cloud retrievals algorithm for MODIS: optical thickness, effective particle radius, and thermodynamic phase, Algorithm Theor. Basis Doc. ATBD-MOD-05, NASA Goddard Space Flight Cent., Greenbelt, Md.
- King, M.D., P. Platnick, G.T. Hubanks, E.G. Arnold, G. Moody and B. Wind, 2006: Collection 005 Change Summary for the MODIS Cloud Optical Property (06_OD) Algorithms. [online]. Available: modisatmos.gsfc.nasa.gov/C005_Changes/C005_CloudOpticalProperties_ver311.pdf
- Koren, I, Y.J. Kaufman, L.A. Remer, and J.V. Martins, 2004: Measurements of the Effect of Amazon Smoke on inhibition of cloud formation. *Science* 27 February 2004: Vol.303.no5662, pp.1342-1345 DOI:10.1126/science.1089424
- Liu, L. and M.I. Mischenko, 2008: Toward unified satellite climatology of aerosol properties: Direct comparisons of advanced level 2 aerosol products. *JQRST* (2008), DOI:10.1016/j.jqrst.2008.05.003.
- Maddux, B.C., S.A. Ackerman, and S. Platnick, 2010: Viewing geometry dependencies in MODIS cloud products. *J. Atmos. Oceanic Technology*, 27, 1519-1528, doi:10.1175/2010JTECHA1432.1
- Marshak, A., S. Platnick, T. Varnai, G. Wen and R.F. Cahalan, 2006: Impact of three-dimensional radiative effects on satellite retrievals of cloud droplet sizes. *J. Geophys. Res.*, 111.D09207, doi:10.1029/2000JD006686

- Meyer, K., S. Platnick, L. Oreopoulos, and D. Lee, 2013: Estimating the direct radiative effect of absorbing aerosols overlying marine boundary layer clouds in the southeast Atlantic using MODIS and CALIOP. *J. Geophys. Res. Atmos.*, 118, 4801–4815, doi:10.1002/jgrd.50449.
- Min, Q., E. Joseph, Y. Lin, L. Min, B. Yin, P. H. Daum, L. I. Kleinman, J. Wang and Y. N. Lee, 2012: Comparison of MODIS cloud microphysical properties with in-situ measurements over the Southeast Pacific. *Atmos. Chem. Phys.*, 12, 11261–11273, 2012
- Nakajima, T., and M. Tanaka, 1986: Matrix formulations for the transfer of solar radiation in a plane-parallel scattering atmosphere. *J. Quant. Spectrosc. Radiat. Transfer.* 35, 13–21
- Nakajima, T., and M. D. King, 1990: Determination of the optical thickness and effective radius of clouds from reflected solar radiation measurements. Part I: Theory. *J. Atmos. Sci.*, 47, 1878–1893
- OMI ATBD, volume 1: OMI Instrument Description and Level 1B Product (2012), http://eosps.gsfc.nasa.gov/eos_homepage/for_scientist/atbd/docs/OMI/ATBD-OMI-01.pdf
- Ott, S.-T., A. Ott, D. W. Martin, J. A. Young, 1991: Analysis of a trans-Atlantic Saharan dust outbreak based on satellite and GATE data. *Mon. Weather Rev.*, 119, 1832–1850
- Painemal, D., P. Zuidema, 2011: Assessment of MODIS cloud effective radius and optical thickness retrievals over the Southeast Pacific with VOCALS-Rex in-situ measurement. *Journal of Geophys. Research*, vol. 116, D24206, doi:10.1029/2011JD016515, 2011
- Platnick, S., King, M. D., Ackerman, S. A., Menzel, W. P., Baum, B. A., Riedi, J. C. and Coauthors, 2003: The MODIS cloud products: Algorithms and examples from Terra. *IEEE Transactions on Geoscience and Remote Sensing*, 41, 459–473.

- Prospero, J.M., 1996: Saharan dust transport over the North Atlantic Ocean and Mediterranean : An overview, in the impact of deserts dust across the Mediterranean, edited by S. Guerzoni, and R. Chester, pp.133-151, Kluwer Acad., Norwell, Mass., 1996b
- Purker, S.J, & V. Klemas, 2011: Remote sensing and global environmental change, Wiley-Blackwell, pp.384
- Ramanathan, V., 1987: The role of Earth radiation budget studies in climate and general circulation research. *J. Geophys. Res.*,92, 4075-4095
- Remer, L.A., Y.J. Kaufman, D. Tanre, S. Mattoo, D.A. Chu, J.V. Martins, R.R. Li, C. Ichoku, R.C. Levy, R.G. Kleidman, T.F. Eck, E. Vermote, B.N. Holben, 2005: The MODIS Aerosol Algorithm, Products and Validation. *J. Atmos. Sci.*,62(4), 947-973
- Roberts, G., M.J. Wooster, and E. Lagoudakis, 2008: Annual and diurnal African biomass burning temporal dynamics. *Biogeosciences Discuss.*, 5,3623-3663
- Rossow, W.B., F. Moshier, E. Kinsella, A. Arking, M. Despois, E. Harrison, P. Minnis, E. Ruprecht, G. Seze, C. Simmer and E. Smith, 1989: ISCCP cloud algorithm intercomparison. *J. Appl. Meteor.*, 24,877-903
- Seethala, C. and A. Horvath, 2010: Global assessment of AMSR-E and MODIS cloud liquid water path retrievals in warm oceanic clouds. *J. Geophys. Res.*, 115,D13202,doi:10.1029/2009JD0126662.
- Stephens, G. L., D.G. Vane., R.J. Boain, G.G. Mace, K. Sassen, Z. Wang and Coauthors, 2002: The CloudSat mission and the A-Train: A new dimension of space-based observation of clouds and precipitation. *Bulletin of the American Meteorological Society*,83, 1771–1790.

- Stowe, L.L., H.Y.M Yeh, T.F. Eck, C.G. Wellemeyer, H.L. Kyle and the Nimbus-7 Cloud Data Processing Team, 1989: Nimbus-7 global cloud climatology. Part II: First year results. *J. Climate*, 2, 671-709
- Textor, C., Schulz, M., Guibert, S., Kinne, S., Balkanski, Y., Bauer, S. and Coauthors, 2006: Analysis and quantification of the diversities of aerosol life cycles within AeroCom. *Chemistry and Physics*, 6, 1777–1813.
- Torres, O., P. K. Bhartia, J. R. Herman, Z. Ahmad, and J. Gleason, 1998: Derivation of aerosol properties from satellite measurements of backscattered ultraviolet radiation: Theoretical basis. *J. Geophys. Res.*, 103, 17 099–17 110.
- Torres, O., P.K. Bhartia, A. Sinyuk, E.J. Welton, and B. Holben, 2005: Total Ozone Mapping Spectroradiometer measurements of aerosol absorption from space: Comparison of SAFARI 2000 ground-based observations. *J. Geophys. Res.*, 110 ,D10S18, doi:10.1029/2004JD004611
- Torres, O., A. Tanskanen, B. Veihelmann, C. Ahn, R. Braak, P.K. Bhartia and Coauthors, 2007: Aerosols and surface UV products from Ozone Monitoring Instrument observations: An overview. *Journal of Geophysical Research*, 112, D24S47, doi:10.1029/2007JD008809.
- Toth, T. D., J. Zhang, J. R. Campbell, J. S. Reid, Y. Shi, R. S. Johnson, A. Smirnov, M. A. Vaughan, and D. M. Winker, 2013: Investigating enhanced Aqua MODIS aerosol optical depth retrievals over the mid-to-high latitude Southern Oceans through intercomparison with co-located CALIOP, MAN, and AERONET data sets, *J. Geophys. Res. Atmos.*, 118, 4700–4714, doi:[10.1002/jgrd.50311](https://doi.org/10.1002/jgrd.50311).
- Twomey, S. and T. Cocks, 1982: Spectral reflectance of clouds in the near-infrared: Comparison of measurements and calculations. *J. meteor. Soc. Japan*. 60, 583-592

- Twomey, S. and T. Cocks, 1989: Remote sensing of cloud parameters from spectral reflectance in the near infrared. *Beitr. Phys. Atmos.* 62,172-179
- Vant-Hull, B., A. Marshak, and L.A. Remer, 2007: The effects of scattering angle and geometry on satellite retrievals of droplet effective radius, *IEEE Trans. GeoSci. Remote Sens.* 45,1039-1045, doi:10.1109/TGRS.2006.890416
- Vaughan, M.S., D. Young, K. Winker, A. Powell, Z. Omar, Y. Liu and C. Hosteler, 2004: Fully automated analysis of space based lidar data:an overview of the CALIPSO retrieval algorithms and data products. *SPIE Int. SOc. Opt. Eng.* , edited by U. Singh, pp.16-30, Maspalamos, Gran Canaria, Spain
- Venkataraman, C. ,G. Habib, A.Eiguren-Fernandez,A.H. Miguel and S.K. Friedlander, 2005: Residential biofuels in South Asia: Carbonaceous aerosol emissions and climate impacts. *Science* 307, 1454(2005):DOI.10.1126/Science.1104359
- Van de Hulst, H.C., 1974: The spherical albedo of a planet covered with a homogenous cloud layer. *Astron. Astrophys.* 35, 209-214
- Wang J. and S.A. Christopher, 2003: Intercomparison between satellite-derived aerosol optical thickness and PM_{2.5} Nass: Implications of Air Quality Studies. *Geophys. Res.*, Vol 30,No.21, 2095, DOI:1.0.1029/2003GK0184174,2003.
- Wetherald, R.T., and S. Manabe, 1988: Cloud feedback processes in a general circulation model. *J. Atmos. Sci.*, 45,1397-1415
- Wilcox, E., M. Harshvardahn, and S. Platnick, 2009: Estimate of the impact of absorbing aerosols over cloud on the MODIS retrievals of cloud optical thickness and effective radius using two independent retrievals of liquid water path. *J. Geophys. Res.*,144, D05210, doi: 10.1029/ 2008JD010589.

- Wilcox, E. M., 2010: Stratocumulus cloud thickening beneath layers of absorbing smoke aerosol. *Atmos. Chem. Phys.*, 10, 11 769–11 777, doi:10.5194/acp-10-11769-2010.
- Yu, H., Y.J. Kaufman, M.Chin, G. Feingold, L.A. Remer, T.L. Anderson and Coauthors, 2006: A review of measurement-based assessments of aerosol direct radiative effect and forcing. *Atmospheric Chemistry and Physics*, 6, 613–666.
- Yu, H., Y. Zhang, H.Chin, Z. Liu, A. Omar, L.A. Remer, Y. Yang, T. Yuan, J. Zhang, 2011: An integrated analysis of aerosol above clouds from A-Train multi-sensor measurements. *Remote Sensing of Environment* 121 (2012) 125–131.